Pharmacological Research 195 (2023) 106891

Contents lists available at ScienceDirect

Pharmacological Research

journal homepage: www.elsevier.com/locate/yphrs

# Administration of intestinal mesenchymal stromal cells reduces colitis-associated cancer in C57BL/6J mice modulating the immune response and gut dysbiosis

Laura Hidalgo-García [a,b,1], Antonio Jesús Ruiz-Malagon [a,b,1], Francisco Huertas [b,c], María Jesús Rodríguez-Sojo [a,b], José Alberto Molina-Tijeras [a,b], Patricia Diez-Echave [a,b], Patricia Becerra [b,d], Benito Mirón [b,e], Rocío Morón [b,f], Alba Rodríguez-Nogales [a,b,*], Julio Gálvez [a,b,g,*], María Elena Rodríguez-Cabezas [a,b,2], Per Anderson [b,h,i,2]

[a] Department of Pharmacology, Center for Biomedical Research (CIBM), University of Granada, 18071 Granada, Spain
[b] Instituto de Investigación Biosanitaria de Granada (ibs.GRANADA), Granada, Spain
[c] Servicio de Cirugía, Hospital Universitario Virgen de las Nieves, 18012 Granada, Spain
[d] Servicio de Anatomía Patológica, Hospital Universitario Clínico San Cecilio, 18014 Granada, Spain
[e] Servicio de Cirugía, Hospital Universitario Clínico San Cecilio, 18016 Granada, Spain
[f] Servicio Farmacia Hospitalaria, Hospital Universitario Clínico San Cecilio, 18016 Granada, Spain
[g] Centro de Investigación Biomédica En Red para Enfermedades Hepáticas y Digestivas (CIBER-EHD), School of Pharmacy, University of Granada, 18071 Granada, Spain
[h] Servicio de Análisis Clínicos e Inmunología, Hospital Universitario Virgen de las Nieves, 18014 Granada, Spain
[i] Departamento de Bioquímica, Biología Molecular e Inmunología III, University of Granada, 18016 Granada, Spain

ARTICLE INFO

*Keywords:*
Mesenchymal stromal cells
Cell therapy
Colorectal cancer
Azoxymethane
DSS colitis
Inflammation
Intestinal microbiota
Dysbiosis

ABSTRACT

*Background:* Patients with inflammatory bowel disease (IBD) have a higher risk of developing colitis-associated colorectal cancer (CAC) with poor prognosis. IBD etiology remains undefined but involves environmental factors, genetic predisposition, microbiota imbalance (dysbiosis) and mucosal immune defects. Mesenchymal stromal cell (MSC) injections have shown good efficacy in reducing intestinal inflammation in animal and human studies. However, their effect on tumor growth in CAC and their capacity to restore gut dysbiosis are not clear.

*Methods:* The outcome of systemic administrations of in vitro expanded human intestinal MSCs (iMSCs) on tumor growth in vivo was evaluated using the AOM/DSS model of CAC in C57BL/6J mice. Innate and adaptive immune responses in blood, mesenteric lymph nodes (MLNs) and colonic tissue were analyzed by flow cytometry. Intestinal microbiota composition was evaluated by 16S rRNA amplicon sequencing.

*Results:* iMSCs significantly inhibited colitis and intestinal tumor development, reducing IL-6 and COX-2 expression, and IL-6/STAT3 and PI3K/Akt signaling. iMSCs decreased colonic immune cell infiltration, and partly restored intestinal monocyte homing and differentiation. iMSC administration increased the numbers of Tregs and IFN-$\gamma^{+}$CD8$^{+}$ T cells in the MLNs while decreasing the IL-4$^{+}$Th2 response. It also ameliorated intestinal dysbiosis in CAC mice, increasing diversity and Bacillota/Bacteroidota ratio, as well as *Akkermansia* abundance, while reducing *Alistipes* and *Turicibacter*, genera associated with inflammation.

*Conclusion:* Administration of iMSCs protects against CAC, ameliorating colitis and partially reverting intestinal dysbiosis, supporting the use of MSCs for the treatment of IBD.

*Abbreviations:* 5-FU, Fluorouracil; AOM, azoxymethane; ASCs, adipose-derived mesenchymal stromal cells; CAC, colitis-associated colorectal cancer; CRC, colorectal cancer; DSS, dextran sulfate sodium; IBD, inflammatory bowel disease; iMSCs, intestinal mesenchymal stromal cells; MLNs, mesenteric lymph nodes; MSCs, mesenchymal stromal cells.

* Corresponding authors at: Department of Pharmacology, Center for Biomedical Research (CIBM), University of Granada, 18071 Granada, Spain
*E-mail addresses:* albarn@ugr.es (A. Rodríguez-Nogales), jgalvez@ugr.es (J. Gálvez).

[1] Both authors contributed equally to the study.
[2] Both authors contributed equally to the supervision of the study.

https://doi.org/10.1016/j.phrs.2023.106891
Received 27 February 2023; Received in revised form 22 July 2023; Accepted 12 August 2023
Available online 14 August 2023

## 1. Introduction

Inflammatory bowel disease (IBD) is a chronic inflammation of the gastrointestinal tract, mainly comprising of Crohn's disease (CD) and ulcerative colitis (UC), with 6.8 million cases globally in 2017 [1]. Although the etiology of IBD is unclear, the disease is characterized by dysregulated innate and adaptive immune responses against a dysbiotic intestinal microbiota [2]. It is well known that chronic inflammation can promote carcinogenesis, exemplified by the connection between IBD and colorectal cancer (CRC) [3]. Eaden et al. showed that CRC risk increases with the duration of IBD, reaching up to 18 % at 30 years after disease onset [4]. Although colitis-associated colorectal cancer (CAC) accounts for only 2 % of all CRC cases, the prevalence of the disease is increasing worldwide. In addition, CAC patients have an earlier onset of disease, a higher frequency of proximal tumors with poorer histopathological differentiation, and shorter survival compared to sporadic CRC patients [5]. Importantly, CAC is the main cause of mortality and reason for surgical intervention in IBD patients [6]. Current treatments of IBD, including anti-TNF-α monoclonal antibodies, reduce the incidence of CAC [7]. However, varying response rates and adverse effects, including a possible promotion of new or recurrent cancers, warrant the search for complementary and/or alternative treatments [8].

Mesenchymal stromal cells (MSCs) are non-hematopoietic, fibroblastic cells found in virtually all organs and tissues, including the bone-marrow, adipose tissue, the intestine and neonatal tissues [9]. MSCs possess potent immunomodulatory and anti-inflammatory properties and ameliorate colitis in animal models [10]. Allogeneic adipose-derived MSCs (ASCs) have been approved by the FDA, the European Medicines Agency, and recently the Japan Ministry of Health, Labor and Welfare for the local treatment of complex perianal fistulas in Crohn's disease patients [11], and efforts are ongoing to establish allogeneic MSCs as a cell therapy also for luminal IBD. However, in vitro-expanded MSCs can adopt protumorigenic properties in vivo. Systemically injected MSCs can incorporate into the tumor stroma, promoting angiogenesis [12], tumor growth [13], and metastatic disease [14]. As IBD patients have a higher risk of developing CAC, it is important to evaluate how MSCs affect tumor growth under such conditions.

To date, only a few studies have addressed the effect of MSC-administrations on inflammation-mediated tumor induction and progression using the azoxymethane (AOM)/dextran sulfate sodium (DSS) model of CAC (Supplementary Fig. 1). This model is based on an initial injection of the genotoxic AOM, usually followed by three cycles of DSS which induces episodes of relapsing/remitting colitis [15]. This model mimics several aspects of inflammation-induced CRC in humans, including elevated levels of COX-2 and iNOS, dense immune cell infiltration, and dysregulation of the K-ras and β-catenin/c-Myc pathways [15,16], as well as a severe disturbance of microbial diversity and relative abundance at the family level, including the families *Ruminococcaceae* and *Akkermansiaceae* [17]. Nasuno et al. showed that simultaneous injection of AOM and syngeneic bone marrow (BM)-MSCs significantly reduced the average tumor number in Lewis rats [18]. Furthermore, some studies have demonstrated that systemic administration of allogeneic BM-MSCs and human umbilical cord-derived MSCs during the first and second DSS-cycle reduce CAC in C57BL/6J mice. In contrast, Hu and colleagues recently showed that TNF-α/IFN-γ-prestimulated MSCs promoted tumorigenesis in the AOM/DSS model [19]. In addition, despite the involvement of the gut microbiota in both protection and induction of colitis, CAC, and CRC [20], only one study has analyzed the effect of MSCs on the dysbiotic gut microbiome in the AOM/DSS model of CAC [21]. Thus, further studies addressing the effects of MSCs on tumor growth and the intestinal microbiota in CAC are necessary.

We have previously demonstrated that human intestinal MSCs (iMSCs) possess tissue-regenerative and immunomodulatory activities both in vitro and in DSS-induced colitis [22]. In this study we wanted to (i) evaluate the effect of delayed iMSC administrations on tumor progression, (ii) further characterize the immunomodulatory effects of iMSCs on both the innate and adaptive immune responses, and (iii) analyze the effect of iMSCs on the microbiota composition using the AOM/DSS model of CAC in C57BL/6J mice.

## 2. Materials and methods

### 2.1. Isolation and culturing of human iMSCs

Intestinal resections were obtained from patients who signed the corresponding informed written consent before undergoing surgery at the University Hospital Virgen de las Nieves (Granada, Spain). These patients had been previously admitted for bowel resection due to colon cancer, benign polyps, or diverticulitis. iMSCs were isolated from non-compromised tissue (i.e., tissue >5 cm distal to the tumor) as described in [22]. iMSCs were cultured in DMEM Advanced supplemented with 10% heat-inactivated fetal bovine serum (FBS) (Gibco), 2 mM ultraglutamine (Lonza), 1 % penicillin/streptomycin (Lonza) and 1 % amphotericin B (Sigma-Aldrich) and maintained at 37 °C and 5 % of $CO_2$ in a Galaxy $R^+$ incubator (RSBiotech). All iMSCs were used at passages 2–8.

### 2.2. AOM/DSS mouse model

All animal studies were carried out in accordance with the "Guide for the Care and Use of Laboratory Animals" as promulgated by the National Institute of Health and the protocols approved by the Ethics Committee of Laboratory Animals of the University of Granada (Spain) (CEEA 17/09/2019/156). Animals were housed in makrolon cages, maintained in an air-conditioned atmosphere with a 12-hour light-dark cycle and provided with free access to tap water and food. Colitis-associated cancer (CAC) was induced in 8–9 weeks old C57BL/6J female mice provided by the Center for Scientific Instrumentation (University of Granada, Granada, Spain) as previously described [15], with some modifications. Briefly, mice were injected i.p. with 10 mg/kg AOM (Sigma-Aldrich). One week later, 2 % (v/v) DSS was added to the drinking water for 5–7 consecutive days, and this was repeated for a total of three DSS cycles with an interval of two weeks between each cycle. iMSCs were administered twice during the development of CAC. iMSCs ($0.5 \times 10^6$ cells in 200 μL of sterile PBS) were injected intraperitoneally (i.p.) at the disease peak of the second and third DSS cycle. Fluorouracil (5-FU), a first-line drug for colorectal cancer treatment was used as a control treatment, being administered 15 mg/kg, by oral gavage, every 3 days, starting at day 48. Disease Activity Index (DAI) was evaluated daily as described in [23]. In brief, weight loss, stool consistency and rectal bleeding were scored using a 0–4 scale, and the DAI was calculated as the mean of the above parameters. On week 14, mice were subjected to a colonoscopy using the Coloview miniendoscopic system (Karl Storz). To this end, mice were anesthetized with isoflurane and the tumor size grade was evaluated as described by Becker et al. [24]. Animals were sacrificed on week 15 and colons were removed, and macroscopically visible tumors were counted and measured. Later, tumor volumes were estimated following the formula $V = (D \times d2 \times \pi)/6$ that calculates the volume of an ellipsoid, where V=volume, D=larger diameter and d=smaller diameter. In addition, representative specimens were taken 1 cm from the rectum and fixed for 24 h in 4% paraformaldehyde. Tissues were dehydrated using increasing concentrations of ethanol and embedded in paraffin for the hematoxylin and eosin staining; or in a sucrose gradient and embedded in OCT to evaluate cell apoptosis and the homing of iMSCs to the intestine. The remaining colonic tissue samples were used for RNA and protein analysis. Spleens, mesenteric lymph nodes (MLNs) and peripheral blood were collected for subsequent analyses as described below.

### 2.3. Gene expression analysis by quantitative PCR (qPCR)

Colonic tissue samples were homogenized using a Precellys 24 tissue homogenizer (Bertin Technologies) and RNA was isolated with the RNeasy® Mini Kit (Qiagen) following the manufacturer's instructions. 1–2 μg of total RNA per sample were reverse transcribed into cDNA using the M-MLV reverse transcriptase, oligo (dT) primers, RNasin® ribonuclease inhibitor and a 10 mM dNTP mix (all from Promega) following the manufacturer's instructions.

Following cDNA synthesis, qPCRs were performed using the MasterMix qPCR SyGreen kit (PCR Biosystems Ltd) in optical-grade 48-well plates, employing an Eco™ Real-Time PCR thermocycler (Illumina). Relative gene expression, using the housekeeping gene glyceraldehyde-3-phosphate dehydrogenase, was calculated by means of ΔΔCt formula and expressed as fold-change (compared to the corresponding control). Specific primer sequences (Sigma-Aldrich) are presented in supplementary table 1 (Supplementary Table 1).

### 2.4. Protein evaluation by Western blot

Colonic samples were cut into pieces and suspended (1:5 w/v) in a lysis buffer containing 20 mM HEPES (pH 7.5), 10 mM EGTA, 40 mM β-glycerophosphate, 2.5 mM $MgCl_2$, 1 % Igepal®, protease inhibitors (1 mM DTT, 2 μg/mL aprotinin, 5 μg/mL leupeptin, 1 mM PMSF, 1 μg/mL iodoacetamide), and phosphatase inhibitors (2 mM sodium orthovanadate, 5 mM sodium fluoride, and 1 mM sodium molybdate) (all from Sigma-Aldrich). Then, tissue homogenates were left for 2 h in a tube rotator at 4 °C. Homogenates were centrifuged at 10,000 × g for 15 min at 4 °C and the protein concentration in the supernatants was determined by the bicinchoninic acid method. The boiled samples (40–60 μg of total protein in 4× Laemmli sample buffer (Bio-Rad)) were resolved by sodium dodecyl sulfate-polyacrylamide gel electrophoresis (SDS-PAGE) under reducing conditions. After gel electrophoresis, proteins were electrotransferred to an immobilon-P PVDF membrane (Sigma-Aldrich). After blocking for 1 h with 5 % non-fat dry milk or 3 % BSA (Sigma-Aldrich) diluted in PBS-T, membranes were incubated overnight with primary antibodies against: iNOS (1:500, BD biosciences, Cat.# 610333), β-catenin (1:1000, Santa Cruz Biotechnology, Cat.# SC-7963), IL-6 (1:500, Cell signaling, Cat.# 12912), Akt (1:1000, Cell signaling, Cat.# 9272), p-Akt (Ser473) (1:1000, Cell signaling, Cat.# 9271), Bax (1:200, Santa Cruz Biotechnology, Cat.# SC-7480), Bcl-2 (1:500, Santa Cruz Biotechnology, Cat.# SC-7382), COX-2 (1:1000, Cell signaling, Cat.# 12282), STAT-3 (1:1000, Cell signaling, Cat.# 4904) and pSTAT3 (Tyr705) (1:1000, Cell signaling, Cat.# 9145). Secondary HRP conjugated antibodies were purchased either from Sigma-Aldrich (1:5000 anti-rabbit IgG, Cat.# A9169) or Cell signaling (1:3000 anti-mouse IgG, Cat.# 7076S) and incubated for 1 h. Control of protein loading and transfer was conducted by detection of β-actin levels with a directly conjugated HRP antibody (1:1000, Santa Cruz Biotechnology, Cat.# SC-47778). Signal development was performed with the Clarity western ECL substrate (Bio-Rad) and signal acquisition using a ChemiDoc image system (Bio-Rad). The quantification of bands was performed by densitometry analysis using either ImageJ (Free Software Foundation Inc) or Image Lab software (Bio-Rad).

### 2.5. Flow cytometry

A flow cytometry analysis of the immune cell composition in peripheral blood, colonic tissue, and MLNs was performed in control, CAC, and CAC+iMSCs groups at the endpoint of the experiment (week 15). On the day of sacrifice, mice were anesthetized with xylazine (10 mg/kg) and ketamine (100 mg/kg) and blood was drained with a 25 gauge heparinized needle and transferred to a tube with anticoagulant, followed by lysis of erythrocytes. Colonic tissue was washed and incubated on a shaker with 5 mL of a prewarmed solution of HBSS (without $Ca^{2+}$ and $Mg^{2+}$) supplemented with 1 mM DTT and 5 mM EDTA for 30 min at 37 °C and 150 rpm. Subsequently, the intestines were washed, cut into pieces, and incubated in DMEM containing 400 U/mL collagenase XI (Sigma-Aldrich, Cat.# C7657), 100 U/mL DNase I (Sigma-Aldrich, Cat.# DN25) and 0.09 U/mL dispase II (Roche Applied System, Cat.# 04942078001) for 40–50 min at 37 °C and 150 rpm. The cell suspensions were passed through a 70 μm presoaked nylon mesh. MLNs were homogenized and the cell suspensions were incubated for 4.5 h (37 °C, 5 % $CO_2$) in 1 mL of medium containing 50 ng/mL PMA (Sigma-Aldrich), 1 μg/mL ionomycin (Sigma-Aldrich) and Brefeldin A (1:1000 dilution, BD Biosciences, Cat.# 555029).

Next, 2–3 × $10^6$ cells/tissue type and mouse were incubated with the live/dead Zombie Aqua fixable viability dye (BioLegend), anti-CD16/32 (BioLegend, Cat.# 101319) and 123 counting eBeadsTM (Invitrogen, Cat.# 01–1234–42), previously diluted in 1× PBS. Samples and fluorescence minus one (FMO) controls were stained for 30 min at 4 °C with specific antibody cocktails for blood (Supplementary Table 2) and intestinal tissue (Supplementary table 3), diluted in FACs buffer (0.1 % BSA and 2 mM EDTA). Subsequently, samples were washed with 1x PBS, fixed with a paraformaldehyde-based solution (Invitrogen, Cat.# 00–8222) and resuspended in 200 μL of FACs buffer. For the MLNs, cells and FMO controls were stained for 30 min at 4 °C with an antibody cocktail diluted in FACs buffer (0.1 % BSA and 2 mM EDTA). In addition, cells from the MLNs were fixed/permeabilized and stained intracellularly for IL-4, IFN-γ, IL-17A and FoxP3 (Supplementary Table 4), using the FoxP3/transcription factor staining buffer set (Invitrogen, Cat.# 00–5523) following the manufacturer's instructions. Data were acquired using a BD FACSymphony™ A5 Cell Analyzer and the results from blood, intestinal tissue and MLNs were analyzed with the Flowjo v10.6.2 software (FlowJo LLC) following gating strategy shown in Supplementary figures 1, 2, and 3, respectively.

### 2.6. Hematoxylin and eosin staining

On the day of sacrifice, representative colonic specimens were taken 1 cm from the rectum and fixed for 24 h in 4 % paraformaldehyde. For the hematoxylin and eosin (H&E) staining, tissues were dehydrated using increasing concentrations of ethanol (70 %, 85 %, 95 % and 100 %), then embedded in paraffin and cut in 5 μm sections. Conventional H&E staining was performed on deparaffinized and rehydrated samples through soaking for 1 min in undiluted Harris Hematoxylin (Casa Álvarez), followed by immersion in 0.5% eosin (Casa Álvarez) for 30 s. Stained slides were then dehydrated in increasing concentrations of ethanol and clarified in xylene before being mounted with DPX media (Casa Álvarez). The tumor slides were evaluated in a blinded fashion by a pathologist.

### 2.7. Assessment of apoptosis by TUNEL assay

On the day of sacrifice, representative colonic specimens were taken 1 cm from the rectum and fixed for 24 h in 4% paraformaldehyde. For immunofluorescence (IF) stainings, samples were dehydrated in a sucrose gradient (first at 15% and then at 30%), embedded in OCT and cut on a cryostat in 8 μm sections. To evaluate cell apoptosis the DeadEnd Fluorometric Tunel system (Promega, Cat.# 3250) was used following manufacturer's indications with some modifications. Briefly, after tissue delimitation, samples were hydrated for 10 min with 1x PBS, followed by tissue permeabilization using proteinase K (20 μg/mL) for 10 min. Next, samples were washed and incubated with equilibration buffer (200 mM dimethylarsinic acid, 25 mM Tris-HCl, 0.2 mM DTT, 0.25 mg/mL BSA and 2.5 mM cobalt chloride) for 10 min before being incubated for 1 h at 37 °C with the rTdT incubation buffer. For negative controls this buffer was prepared without the rTdT enzyme. After 1 h, sections were washed with 2× saline sodium citrate (SSC) buffer for 15 min and then three times with 1x PBS. Finally, Hoechst 33342 (Invitrogen) was used to stain nuclei and samples were mounted with ProLong™ glass antifade mountant (Invitrogen). Images were acquired on a LEICA

DM5500 fluorescence microscope (Center for Scientific Instrumentation, University of Granada, Granada, Spain). Acquisition of the blue and green channels (positive signal) was performed using the A and I3 filter cubes, respectively. Quantification of $TUNEL^+$ cells/field was done using 5 random fields per slide. Images were then analyzed with ImageJ software (Free Software Foundation Inc.).

### 2.8. Assessment of the homing of iMSCs to the intestine

To assess iMSC homing in colon samples, paraformaldehyde fixed 8 μm tissue sections were hydrated for 10 min in 1× PBS, and treated with a solution containing 0.1 % saponin, 1 % BSA and 0.05 % sodium azide for 1 h at room temperature. Then, slides were incubated with the anti-nuclei antibody conjugated with AF488 (1:100 dilution, Sigma-Aldrich, Cat.# MAB1281A4) at 4 °C overnight. The following day, sections were washed three times with 1x PBS and all nuclei were counterstained with Hoechst 33342 (Invitrogen). As a positive control, iMSCs were grown in a Nunc Lab-Tek Chamber slide™, fixed in 4 % paraformaldehyde in PBS (pH 7.4) for 15 min at room temperature and washed thrice with 1× PBS. Then, cells were permeabilized and blocked with a 0.1 % saponin, 1 % BSA solution for 1 h, followed by staining with the anti-nuclei antibody conjugated with AF488 (1:100 dilution) at 4 °C overnight. Slides were mounted with ProLong™ glass antifade mountant (Invitrogen) and a 1.5 mm coverslip. Images were taken on a confocal laser microscope ZEISS LSM900 of the Unit of Optical Microscopy and Cellular Imaging of the ibs.GRANADA. Samples were excited with the 405-nm solid-state laser for visualization of Hoeschst labeling and the 488-nm laser for AF488 labeling. Images were captured using a 20× dry objective with a numerical aperture of 0.8.

### 2.9. Microbiome analysis

Colonic luminal contents were collected from all mice at the end of the treatment and kept immediately at − 80 °C until DNA extraction. Total DNA was isolated following the procedure described by Rodriguez-Nogales et al. [25]. PCR amplification of the targeted regions was performed by using "fusion primers", targeting 16S V4-V5 regions with multiplexing on the Illumina MiSeq machine (Illumina Inc.). The PCR products with proper size were selected by 2 % agarose gel electrophoresis. The same amount of PCR products from each sample were then pooled to make one library to be quantified fluorometrically before sequencing. After the sequencing was completed, all reads were scored for quality, and any poor quality and short reads were removed.

For microbiome analyses, paired-end reads were assigned to samples based on their unique barcodes and truncated by cutting off the barcode and primer sequences. Paired-end reads were merged using FLASH (V1.2.7) [26]. Quality filtering on the raw tags were performed to obtain the high-quality clean tags [27] using the Qiime (V1.7.0) quality-controlled process [28]. The tags were compared with the SILVA reference database using UCHIME algorithm [29] to detect and remove chimera sequences [30]. Lastly, the Effective Tags were obtained. With the effective tag were obtained the OTU cluster and Taxonomic annotation using Uparse software [31]. Sequences with ≥ 97 % similarity were assigned to the same OTUs. Representative sequence for each OTU was screened for further annotation. For each representative sequence, Qiime in Mothur method was performed against the SSU rRNA database of SILVA Database [32] for species annotation at each taxonomic rank [33]. OTUs abundance information were normalized using a standard sequence number corresponding to the sample with the least sequences. Subsequent analysis of alpha diversity and beta diversity were all performed based on this output normalized data. Alpha and beta diversity was calculated with QIIME and displayed with R software (Version 2.15.3).

### 2.10. Statistical analysis

Statistical analysis was performed using the GraphPad Prism version 7 software (GraphPad Software). Data are represented as mean(SEM), or as box plots showing the median (middle line), ± SEM range, and extreme values (whiskers) of at least 3 independent experiments/biological replicates unless otherwise stated in the figure legends. The Mann–Whitney U-test for non-parametric data was used for the analysis of the DAI and microscopic score. For the rest of the data, multiple comparisons between groups were performed using the one-way ANOVA, followed by the Bonferroni post hoc test. A P-value $< 0.05$ was considered significant. We employ a letter-based system where groups with different letters show statistical significance ($P < 0.05$), whereas groups that share the same letter do not differ statistically.

## 3. Results

### 3.1. iMSC administrations reduce disease severity in the AOM/DSS model of CAC

CAC was induced in C57BL/6J female mice (CAC control) (n = 13) by the injection of AOM followed by three cycles of DSS (2 % w/v) (Fig. 1A). One group of CAC mice (CAC+iMSCs) (n = 13) was injected with iMSCs ($0.5 \times 10^6$ iMSCs/mouse i.p.) at the end of the 2nd and 3rd DSS cycle. One group of CAC mice (CAC+5-FU) (n = 13) was administered orally every 3 days with 5-FU, a standard colorectal cancer drug, as a treatment control. The control mice (control) (n = 12) were not injected with AOM and received water instead of DSS (Fig. 1A). During the three DSS cycles, weight loss and DAI were monitored as described in the materials and methods section. CAC control mice showed an important weight loss and an increase in DAI during each DSS cycle (Fig. 1B). The first systemic administration of iMSCs did not affect weight loss or the DAI. However, a decrease in weight loss and DAI was observed during the third DSS cycle in the iMSC-treated group, even before the second iMSC administration. These data suggest that the first iMSC administration was able to induce protection against subsequent DSS-induced inflammation and tissue injury (Fig. 1B). The disease ameliorating effects of the iMSC administrations persisted for seven weeks after the last DSS administration, until the end of the experiment, as reflected by a significant reduction in spleen weight (Fig. 1C) and colon weight/length ratio (Fig. 1D). In contrast, 5-FU did not alleviate weight loss or DAI (Fig. 1B), nor reduce the spleen weight (Fig. 1C) in CAC mice but diminished the colon weight/length ratio (Fig. 1D).

### 3.2. iMSC administrations reduce the number and size of colonic tumors in CAC mice

In the AOM/DSS CAC model, aberrant crypt foci can be seen about two weeks after the initial AOM injection, while macroscopically visible lesions can be observed from week 3–4 [15]. A week before the sacrifice of the mice, the extent of colitis and tumor development was evaluated by colonic endoscopy (n = 4–5/group), using a scoring system developed by Becker et al. [24], as described in the materials and methods section. Both CAC+iMSCs and CAC+ 5-FU mice exhibited a significantly reduced tumor size grade (Fig. 2A and B) compared to CAC control mice. After sacrifice, colons were opened longitudinally and tumor load, size and volumes were measured and calculated as detailed in the materials and methods section. AOM/DSS-induced tumors were located in the distal part of the colon and rectum (Fig. 2C), which is in line with the predominant localization of inflammation-induced intestinal tumors in human IBD patients. We observed that CAC+iMSCs and CAC+ 5-FU mice had significantly fewer tumors compared to CAC control mice (Fig. 2D). In contrast to other studies [18, 21, 34–36], the tumors in CAC+iMSCs mice were significantly smaller compared to those found in CAC control mice (Fig. 2E, F, and G).

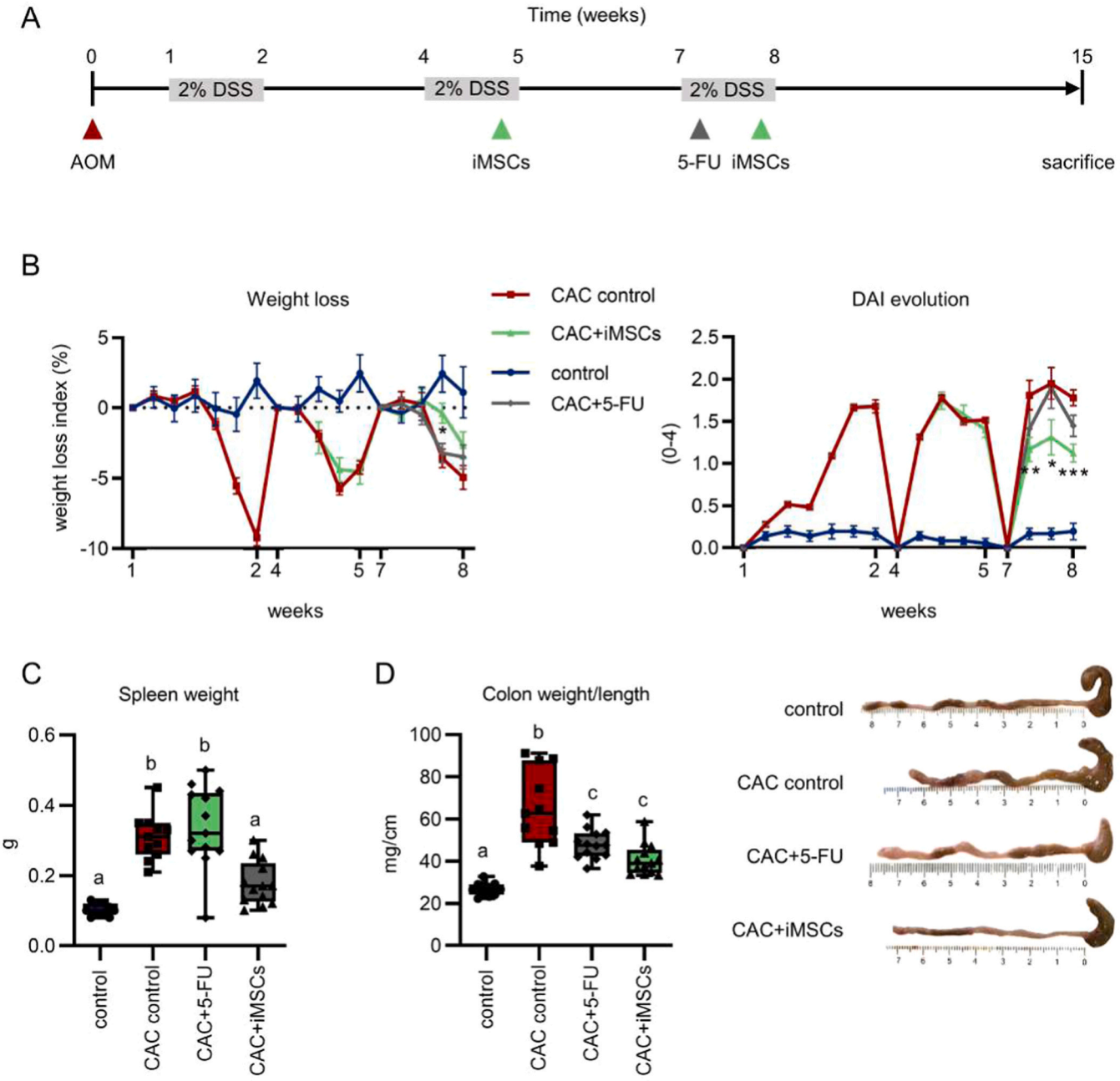


**Fig. 1.** iMSC administrations ameliorate colitis in the AOM/DSS model. (A) To induce the development of CAC, mice (n = 13; CAC) were injected i.p. with 10 mg/kg of AOM. One week later, mice were subjected to three cycles of 2 % DSS in the drinking water ad libitum for 5–7 days, followed by two weeks of sterile water. iMSCs ($0.5 \times 10^6$/mouse) were injected i.p. (n = 13) at the peak of the second and third cycles of DSS. 5-FU (15 mg/kg) was administered (n = 13) by oral gavage every 3 days starting on day 48. Mice receiving tap water were used as control mice (n = 12). (B) Weight loss index (left) and disease activity index (DAI) (right) were determined daily during the three DSS cycles. (C) Spleen weight and (D) colon weight/length were determined on week 15. Representative images of the colons of control, CAC control, CAC+ 5-FU and CAC+MSCs mice are shown (right). Data are expressed as mean(SEM). *=P < 0.05, **=P < 0.01, ***=P < 0.001 CAC control mice vs. CAC+iMSCs. Different groups with different letters (a-c) show significant differences (P < 0.05).

### *3.3. iMSCs inhibit tumor development and do not engraft in the inflamed colon*

On the day of sacrifice, representative colonic specimens (n = 6/group) were taken 1 cm from the rectum, and transversal colon sections were stained with hematoxylin and eosin (H&E) and assessed in a blinded fashion by a pathologist. In general, tumors were classified as polypoid adenocarcinomas in situ, exhibiting epithelial loss of polarity, a cribriform pattern with intraglandular necrotic debris (Fig. 3A). Tumor invasion into muscularis mucosae was only evident in two samples (one from the CAC control group, and one from the CAC+iMSCs group). In the CAC control mice, at least one polypoid adenocarcinoma covering almost the whole colonic lumen was found in 5 out of 6 animals and in CAC+ 5-FU mice 4 out of 5, whereas only one out of 6 CAC+iMSCs mice presented a tumoral mass in the corresponding tissue segment (data not shown). Regarding inflammation, CAC control mice exhibited a lower number of goblet cells combined with larger areas of edema, ulceration and lymphoplasmacytic infiltration compared to CAC+iMSCs and 5-FU mice. However, despite the reduction in inflammation and tumor burden in CAC+iMSCs mice, using a human nucleus-specific antibody, we could not detect iMSCs in the colon at the day of sacrifice (Fig. 3B). Furthermore, using the TUNEL assay we found that

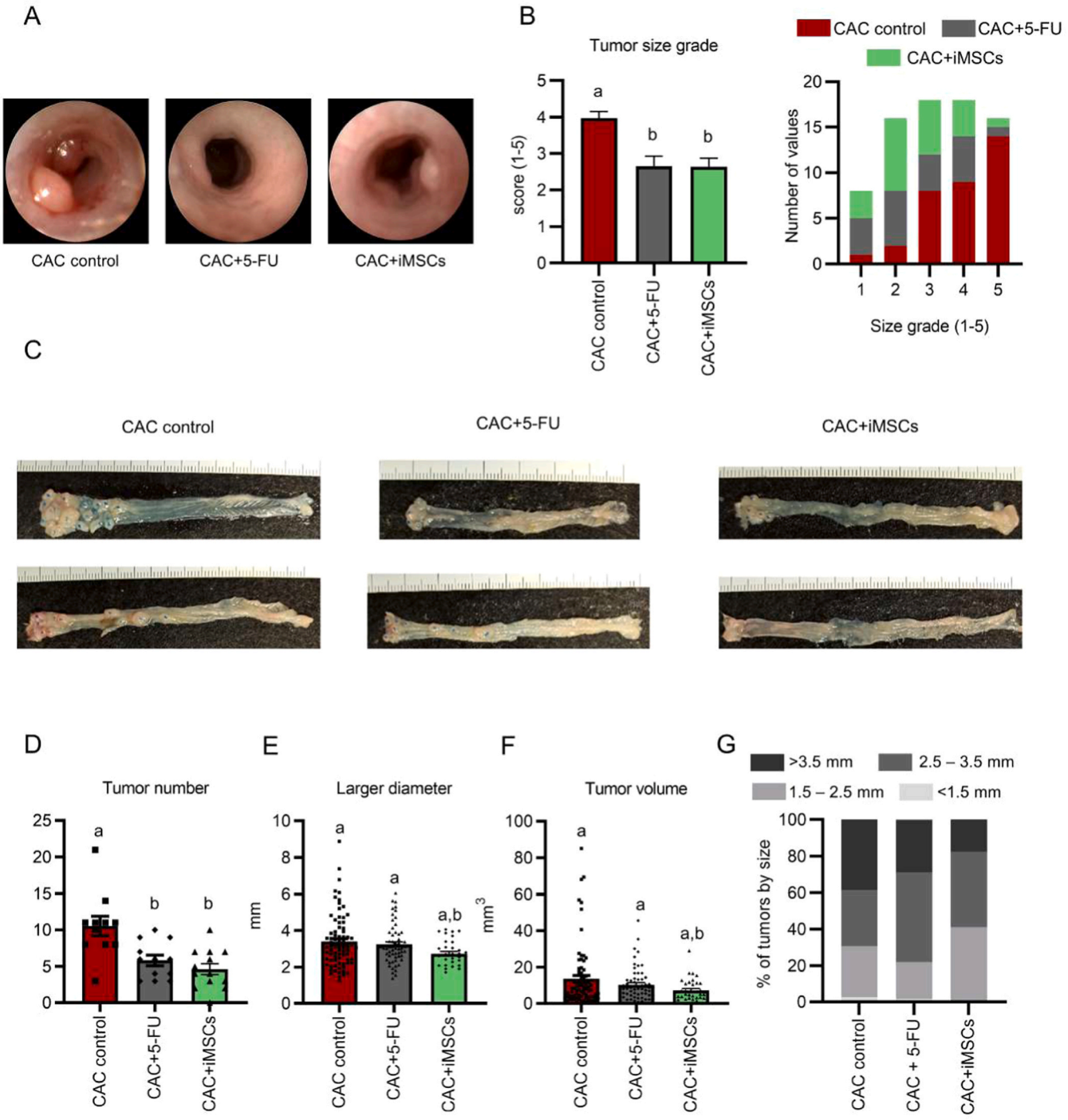


**Fig. 2.** iMSC administrations reduce tumor number/size in AOM/DSS-treated mice. (A) One week before sacrifice, colonoscopy was performed in 4–5 mice/group. Representative images from CAC control, CAC+ 5-FU and CAC+iMSCs mice are shown (left) and the tumor size grade (right) and (B) colitis severity was analyzed based on the colonoscopies as described in the materials and methods. (C) Representative images of colons removed from CAC control (left), CAC+ 5-FU (middle) and CAC+iMSCs (right) mice. Subsequently, (D) tumor number, (E) tumor larger diameter, (F) tumor volume and, (G) tumor size distribution was assessed. Values are represented as mean(SEM). Groups with distinct letters (a-b) show significant differences ($P < 0.05$).

apoptotic cell death was significantly higher in CAC+ 5-FU mice compared to healthy controls, CAC control mice and CAC+iMSCs mice. These data are in agreement with the potent cytostatic effect of 5-FU (Fig. 3C).

### *3.4. iMSC administration downregulates the expression of inflammatory mediators and signaling pathways that drive tumorigenesis in CAC*

We next analyzed the gene expression of several immune/inflammatory mediators in the colon that promote CAC in the AOM/DSS model and in IBD patients. The proinflammatory cytokines *Il-6* and *Tnf-α* were significantly increased in CAC control mice, whereas iMSC-treated mice exhibited reduced levels of both cytokines (Fig. 4A). Similarly, *Il-17* and

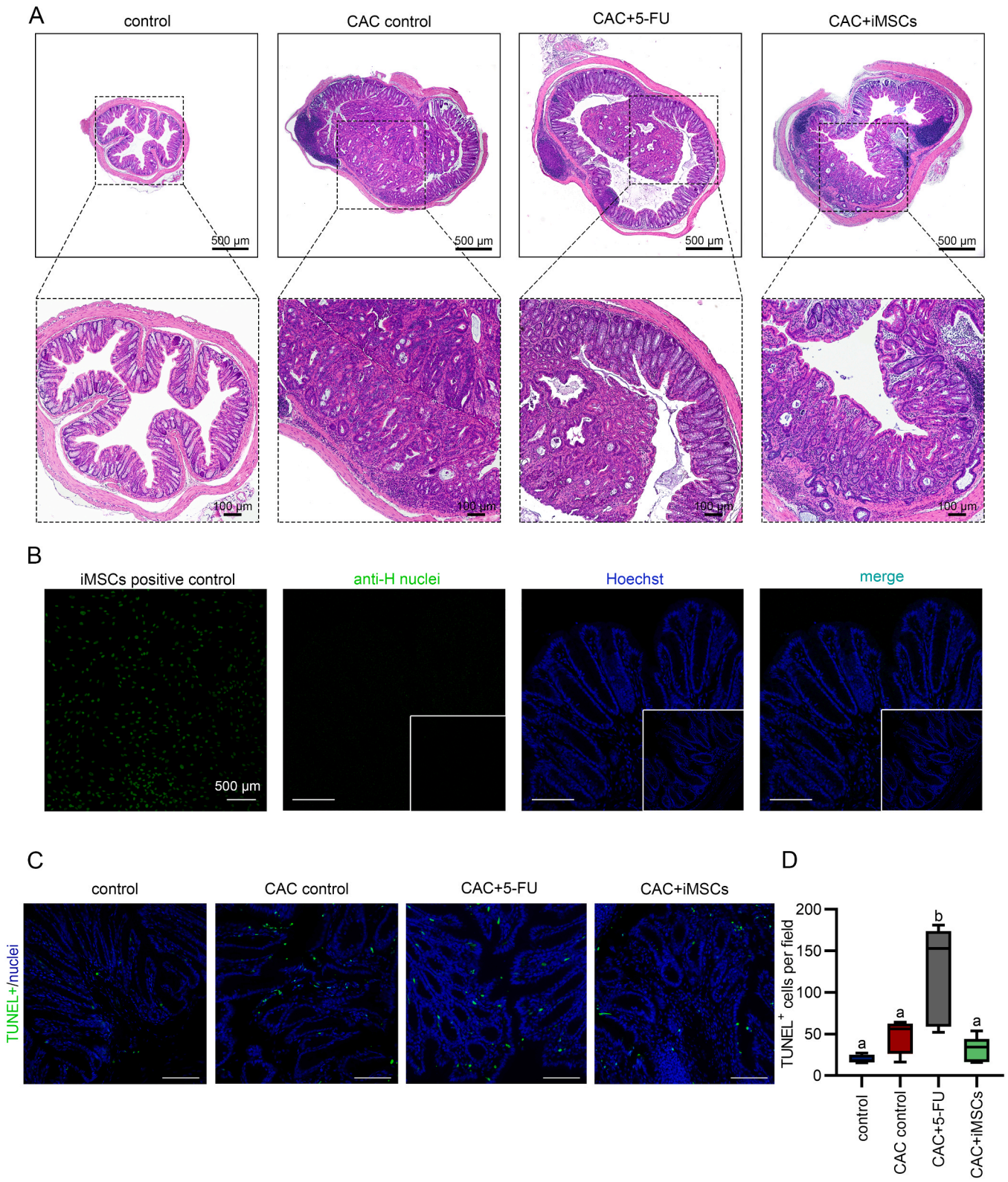


**Fig. 3.** iMSCs inhibit tumor development and do not engraft in the inflamed colon. (A) Representative images of paraffinized transversal sections of colons from control, CAC control and CAC+MSCs mice stained with hematoxylin and eosin taken at different magnifications (4x and 10x). (B) Representative images of iMSCs grown on a chamber slide (left; iMSCs positive control), and colonic tissue sections from a CAC+iMSCs mouse stained with the anti-human nuclei-specific antibody (anti-H nuclei), with Hoechst 33342 (Hoechst), and their overlay (merge). Smaller images represent CAC control mice as negative controls). (C) Representative images of TUNEL stained colon sections from control, CAC control, CAC+ 5-FU, and CAC+iMSCs experimental groups showing apoptosis. Apoptotic cells are stained in green and nuclei in blue (Hoechst 33342). (D) The graph shows TUNEL$^{+}$ cells/field, and data are represented as ± SEM range, median (middle line) and extreme values (whiskers) of 4–5 mice/group. Groups with different letters (a-b) show significant differences ($P < 0.05$). The white line represents 500 μm.

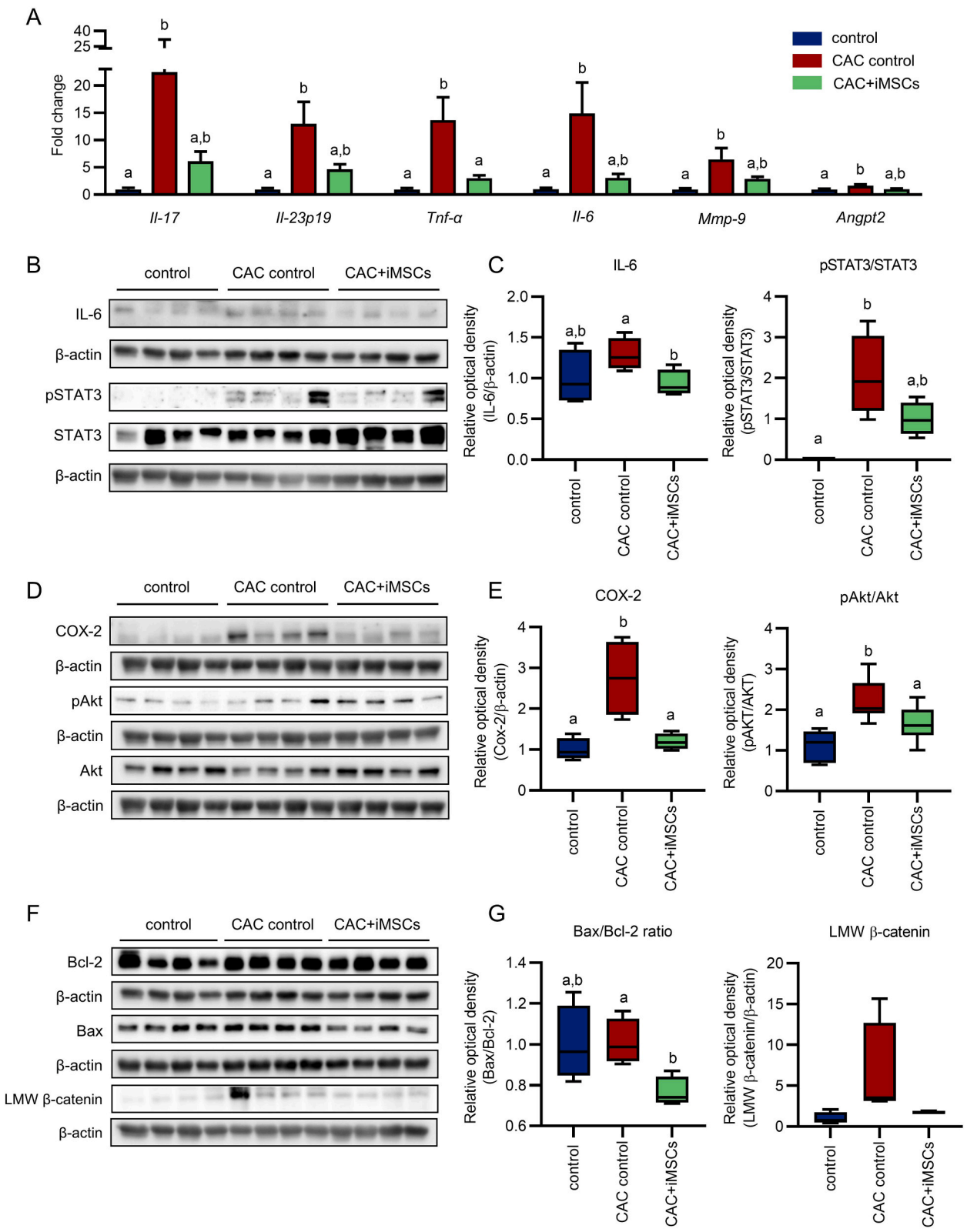


**Fig. 4.** iMSCs downregulate the expression of several key molecules/pathways that drive CAC development and progression in AOM/DSS mice. (A) Total RNA was extracted from colons from control, CAC control and CAC+iMSCs mice collected on the day of sacrifice and the gene expression of *Il-17*, *Il-23-p19*, *Tnf-α*, *Il-6*, *Mmp-9* and *Angpt2* was assessed by RT-qPCR. Data are expressed as mean(SEM) of fold change relative control mice (n = 8 mice/group). Protein expression of IL-6, pSTAT3, STAT3 (B), COX-2, pAkt, Akt (D), and Bcl-2, Bax and LMW β-catenin (F) in colonic protein extracts from control, CAC control and CAC+iMSCs mice were analyzed by Western blot. The relative optical densities for the different proteins were calculated using β-actin as loading control, except for the pSTAT3/STAT3 and pAkt/Akt ratios (C, E, and G). Box plots represent ± SEM range, median (middle line) and extreme values (whiskers). Groups with different letters (a-b) exhibit statistically significant differences ($P < 0.05$). Graphs without letters reflect no significant differences between groups.

*Il-23* (p19 subunit), which are known to promote CAC development [37], were significantly upregulated in CAC control mice in comparison to healthy controls, with a lower expression in iMSC-treated mice (Fig. 4A). In addition, the IL-23-inducible gene matrix metalloproteinase-9 (*Mmp-9*), and angiopoietin-2 (*Angpt-2*), both prognostic factors associated with poor survival in CRC [38,39], were reduced in CAC+iMSCs mice in comparison to CAC control mice (Fig. 4A).

In the AOM/DSS mouse model, high IL-6 and COX-2 levels activate the JAK1/2/STAT-3 and PI3K/Akt signaling pathways, leading to an increased tumor cell proliferation and resistance to apoptosis, thereby increasing tumor growth. A Western blot analysis of colonic protein lysates revealed an increase in IL-6, and COX-2 expression and an activation of both the STAT3 and Akt signaling pathways in control CAC mice compared to control animals (n = 4/group) (Fig. 4B, C, D and E). In contrast, CAC+iMSCs mice exhibited significantly reduced IL-6 and COX-2 expression and Akt signaling, with a similar, but non-significant decrease in STAT3 phosphorylation (Fig. 4B-E). Furthermore, we detected an increase, albeit not significant, of the CRC-associated low-molecular weight (LMW) β-catenin [40] in CAC control mice when compared to control and CAC+iMSCs mice (Fig. 4F and G, right graph). Finally, the Bax/Bcl-2 ratio was elevated in CAC control mice in comparison to the CAC+iMSCs group, indicating augmented levels of apoptosis in CAC colonic cells. Taken together, our data suggest that iMSCs can prevent the inflammation-induced induction and activation of tumorigenic factors and signaling pathways.

### 3.5. *iMSC administrations reduce the CAC-induced increase in blood inflammatory Ly6C$^{hi}$MHCII$^{-}$CCR2$^{+}$ monocytes*

Next, we aimed to characterize the mechanisms by which iMSCs can decrease the AOM/DSS-induced CAC development, focusing on peripheral and local immune responses. Monocytes and macrophages play important roles in promoting inflammation and tumorigenesis in CAC [41]. Thus, we evaluated the composition of monocytic subpopulations in peripheral blood of control, CAC control and CAC+iMSCs mice (n = 5/group) at the end of the experiment by flow cytometry as described in the materials and methods section.

We detected an increase in circulating CD11b$^{+}$ myeloid cells in CAC control mice, compared to control and CAC+iMSCs mice (Fig. 5A, and

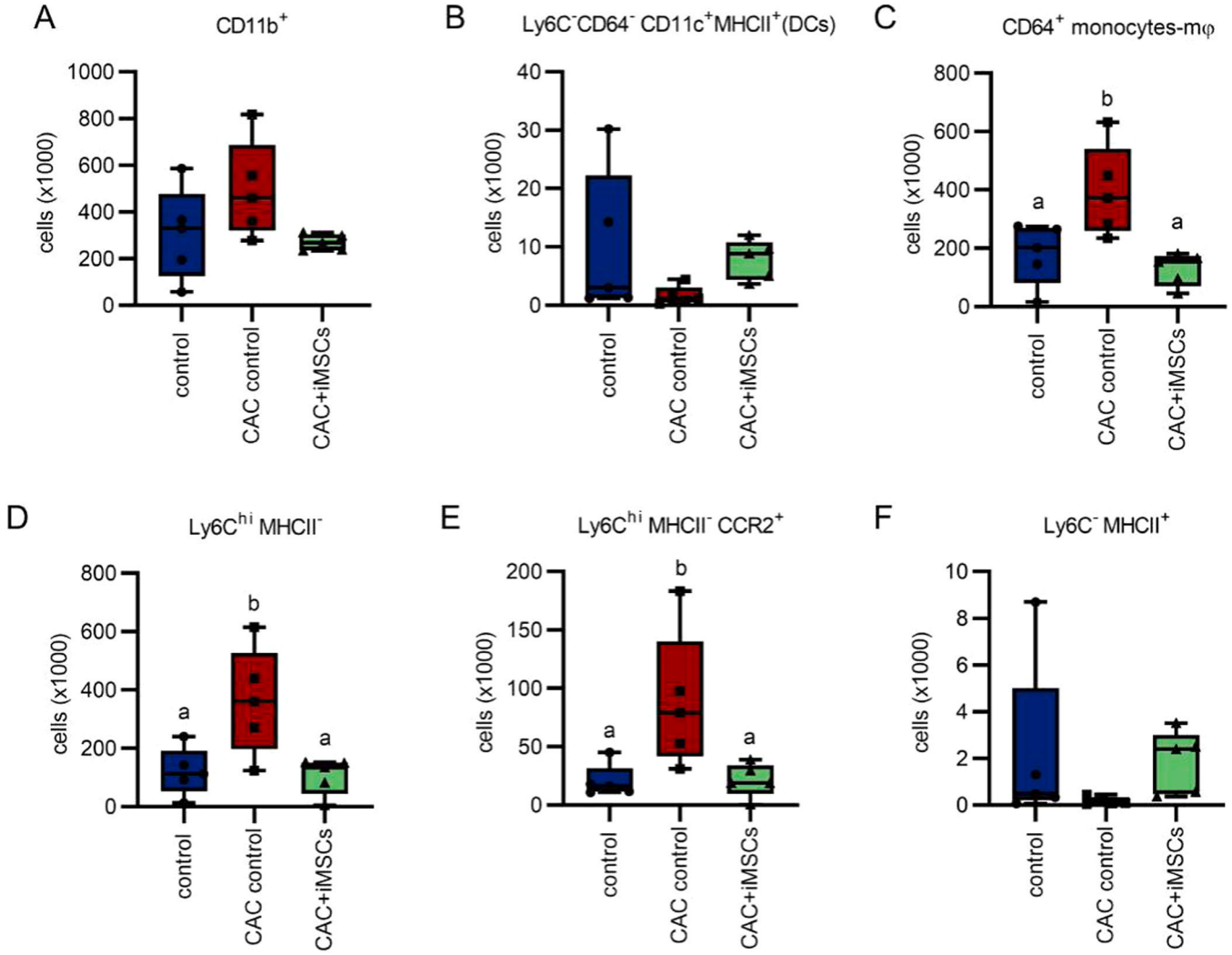


**Fig. 5.** iMSC administrations reduce the numbers of inflammatory monocyte subpopulations in the blood of AOM/DSS mice**.** Peripheral blood from control, CAC control and CAC+iMSCs mice (n = 5 mice/group), collected at the end of the experiment, were analyzed for monocyte subpopulations and dendritic cells by flow cytometry as described in the materials and methods and supplementary information. Total number of (A) CD11b$^{+}$ myeloid cells, (B) Ly6C$^{-}$CD64$^{-}$CD11c$^{+}$MHCII$^{+}$ dendritic cells (DCs), (C) CD64$^{+}$ monocytes-macrophages, (D) Ly6C$^{hi}$MHCII$^{-}$ monocytes, (E) CCR2$^{+}$Ly6C$^{hi}$MHCII$^{-}$, and (F) Ly6C$^{-}$MHCII$^{+}$ non-classical monocytes present in the three experimental groups. Box plots represent ± SEM range, median (middle line) and extreme values (whiskers). Groups with different letters (a-b) exhibit statistically significant differences (P < 0.05). Graphs without letters reflect no significant differences between groups.

B). The CD11b$^+$ population consisted mainly of CD64$^+$ cells of the monocyte-macrophage lineage and not of CD64$^-$CD11c$^+$dendritic cells (Fig. 5B and C). During homeostasis, Ly6C$^{hi}$MHCII$^-$ monocytes are known to home to the intestine in a CCR2/CCL2-dependent manner. Once in the lamina propria, they mature and ensure the replenishment of tissue-resident macrophages [42]. We detected an increase of classical Ly6C$^{hi}$MHCII$^-$ inflammatory monocytes (Fig. 5D), also expressing CCR2 in CAC control mice in comparison to control and CAC+iMSCs animals (Fig. 5E). Thus, the accumulation of this population confirms a higher level of inflammation in CAC control mice and supports the antiinflammatory activity of iMSCs. In addition, although no significant differences were found, marked tendencies appeared in other relevant immune populations such as dendritic cells (Fig. 5B) or non-classical Ly6C$^-$MHCII$^+$ macrophages (Fig. 5F). In both cases, iMSC-treated mice presented cell numbers similar to those found in control mice.

### 3.6. iMSC administration reduces granulocyte infiltration and partially restores macrophage differentiation in the colons of CAC mice

We next analyzed the immune cell composition in the colons of control, CAC control, and CAC+iMSCs mice by flow cytometry. Consistent with the increased colon weight/length ratio in CAC control mice (Fig. 1D), the total number of intestinal cells was also higher (mean (SEM)= $16 \times 10^6$( $\pm 3.8 \times 10^6$) cells) in comparison with healthy controls (mean(SEM)= $3.8 \times 10^6$( $\pm 0.13 \times 10^6$) cells) and the iMSCs treated group (mean(SEM)= $6.9 \times 10^6$ ( $\pm 1.5 \times 10^6$) cells). Regarding the colonic immune infiltrate, we observed an increase in total CD45$^+$ immune cells in the CAC group compared to control mice (Fig. 6A), including CD11b$^+$ myeloid cells (Fig. 6B), neutrophils (CD45$^+$/CD11b$^+$/Ly6G$^+$) (Fig. 6C), and eosinophils (CD45$^+$/CD11b$^+$/Ly6G$^-$/MHCII$^-$/SSC$^{hi}$) (Fig. 6D). In addition to monocytes/macrophages, both neutrophils and eosinophils can promote intestinal inflammation and CAC [43,44]. Interestingly, administrations of iMSCs reduced the infiltration of all the above immune cells, which correlated with the reduced inflammation and tumor burden in these mice (Fig. 6B, C, and D).

As previously mentioned, in steady state conditions, Ly6C$^{hi}$MHCII$^-$ monocytes migrate to the intestine where they differentiate into anti-inflammatory mature Ly6C$^-$MHCII$^+$ macrophages, through a process known as the monocyte "waterfall" [42] (Fig. 6E, left dot plot). However, in colitis this local maturation is dysregulated, resulting in the accumulation of pro-inflammatory Ly6C$^{hi}$MHCII$^-$ macrophages with a M1-like inflammatory phenotype (Fig. 6E, center dot plot) [45]. We found that the administration of iMSCs almost restored the balance of newly recruited (Ly6C$^{hi}$MHCII$^-$) to mature (Ly6C$^-$MHCII$^+$) macrophages in the colon, similar to that of healthy mice (Fig. 6E right dot plot; and Fig. 6G, and H). Furthermore, we observed an increase in M1 (CD86$^+$ with variable expression of F4/80, MHCII and Ly6C) immature macrophages in the CAC control mice in comparison to control and CAC+iMSCs mice (Fig. 6F). In contrast, the numbers of tissue resident-like Ly6C$^-$MHCII$^+$CD206$^+$ macrophages (Fig. 6I) were higher in CAC+iMSCs mice, in comparison with both control groups. In summary, our data highlight that the therapeutic capacity of iMSCs in CAC correlates with their ability to inhibit granulocyte infiltration and restore the monocyte "waterfall" in the inflamed colon.

### 3.7. iMSC administration reduces the Th2 compartment, while increasing the numbers of Th17, Tregs, and Tc1 cells in the MLNs of CAC mice

We next analyzed the proportion and cytokine production by CD4$^+$ and CD8$^+$ T cells in the MLNs of control, CAC control and CAC+iMSCs mice (n = 5/group) by flow cytometry, as detailed in the materials and methods section. We observed a substantial increase in CD4$^+$ T cells producing IFN-γ (Th1), IL-4 (Th2), and IL-17 (Th17) in CAC control mice compared to healthy control mice (Fig. 7A-D). In comparison to CAC control mice, iMSC-treated mice showed reduced numbers of Th2 cells, similar Th1 levels (Fig. 7B and C), and an increase in both Th17 cells (Fig. 7D) and Tregs (Fig. 7F). An increased Th17/Treg ratio is associated with an exacerbated inflammation and has been described in IBD patients [46]. This agrees with the increased Th17/Treg ratio observed in CAC control mice, and its reversal to control levels in iMSC-treated mice (Fig. 7G). Interestingly, we observed a significant increase in the numbers of CD8$^+$ T cells and CD8$^+$IFN-γ$^+$ Tc1 cells in CAC+iMSCs mice, in comparison to both control and CAC mice (Fig. 7H, and I).

### 3.8. iMSC administration ameliorates gut dysbiosis in CAC mice

Finally, we analyzed the effect of iMSC treatment on the gut microbiota since dysbiosis can drive intestinal inflammation and promote CRC [47]. The distribution histogram shows the key role of microbiome abundance. In this sense, all bacterial phyla were modified among experimental groups. The microbiome composition in CAC control mice revealed an increase in the relative abundance of *Actinobacteria* (recently renamed as *Actinomycetota), Bacteroidetes* (now renamed as *Bacteroidota),* and *Verrucomicrobia,* while the *Bacillota* (previously called *Firmicutes*) and *Proteobacteria* (recently renamed as *Pseudomonadota)* were reduced in comparison to control mice (Fig. 8A, left graph). The administration of iMSCs partially reversed the abundances of these phyla. Thus, *Bacteroidota, Actinomycetota, Pseudomonadota,* and *Verrucomicrobia* returned to control levels, while the effect on the relative abundance of *Bacteroidota* was less evident (Fig. 8A, left graph). Furthermore, CAC control mice showed a significantly reduced *Bacillota* to *Bacteroidota* (Bacillota/Bacteroidota) ratio when compared with control mice (Fig. 8A, right graph). Interestingly, the iMSC treatment was able to increase this ratio (Fig. 8A, right graph). On the other hand, microbiota structure beta diversity (β-diversity) was analyzed with weighted UniFrac principal coordinate analysis (PCoA). The gut microbiota in CAC+iMSCs mice showed similarity and presented an overlap between the CAC control and control groups (Fig. 8B). Additionally, the Chao1 richness estimator, Shannon index and the Observed species were measured to evaluate the richness and the alpha diversity (α-diversity) of the microbiota. As shown in Fig. 8C, all α-diversity indices of the CAC control group were significantly lower than those of the control group ($P < 0.05$), while a significant restoration was observed in iMSC-treated mice (Fig. 8C). As shown in Fig. 8D, a Venn diagram was also determined, which is commonly used to display the gut microbiota overlap between groups. The Venn diagram indicates the number of operational taxonomic units (OTUs) which were common and unique to each experimental group. The total number of OTUs in this study was 1108, in which the OTU number of the control group was higher than those of the CAC control group (50 vs 33) (Fig. 8D). Interestingly, the highest number of OTUs was observed in iMSC-treated mice (Fig. 8D). The Venn diagram also showed a larger overlap between the control and CAC+iMSCs group (75 OTUs) compared with the CAC control and CAC+iMSCs group (68 OTUs) (Fig. 8D). These results indicate that the gut microbiota of control mice is more similar to that of the CAC+iMSCs group. Lastly, we explored the taxonomic signatures at the genus level. Genera with average abundance levels > 0.5 % (35 genera) in the three groups were used to construct the heatmap. Twenty-five of the 35 genera were observed to have significant differences in abundance between control and CAC control mice (Fig. 8E). The CAC control group exhibited a greater abundance of *Clostridium*, *Turibacter*, *Clostridia_UCG-014*, *Romboustia*, *Alistipes*, *Bifidobacterium*, *Prevotellaceae*, *Dubosiella*, *Lactobacillus*, *Enterorhabdus*, *Lachnospiraceae*, *Rikenellaceae*, *Odoribacter*, *Parabacteroides*, *Faecalibaculum*, *Eubacterium_fissicatena*, *Aureispira*, *Colidextribacter* and *Bacteroides* and a decreased abundance of *Ileibacterium*, *Coriobacteriaceae*, *Muribaculaceae*, *Ruminococcus* and *Desulfovibrio* compared with control group (Fig. 8E). The iMSCs treatment was able to partially restore all genera modified in CAC control group except *Prevotellaceae_UCG-006*, *Dubosiella*, *Lactobacillus*, *Muribaculum*, *Parasutterella*, *Alloprevotella*, *Muribaculaceae*, *Ruminococcus*, and *Desulfovibrio* (Fig. 8E).

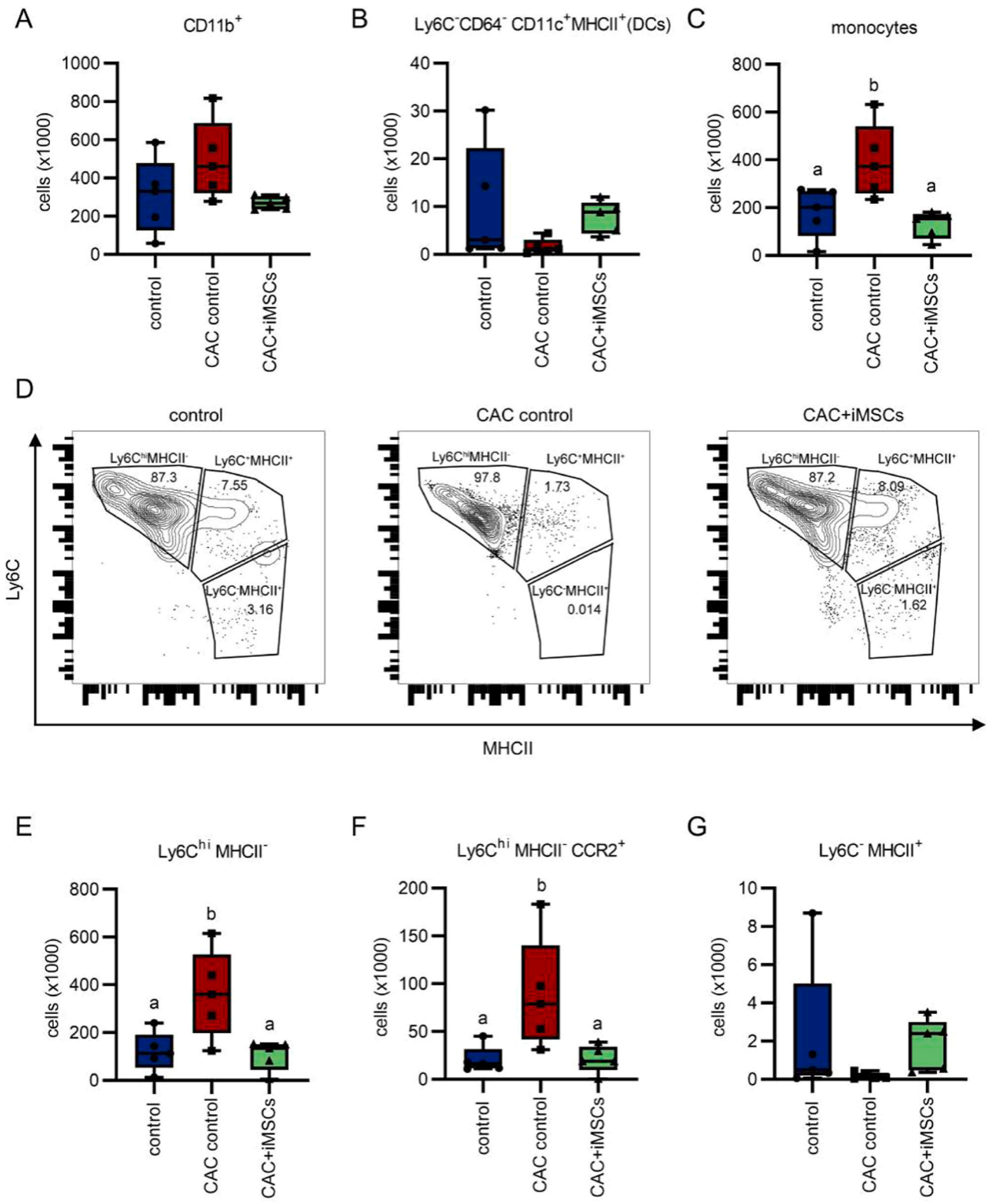


**Fig. 6.** iMSC administrations reduce granulocyte infiltration and partially restore macrophage differentiation in the colons of CAC mice**.** Colons from control, CAC control and CAC+iMSCs mice (n = 3–4 mice/group) were collected at the end of the experiment, and granulocytes and monocyte/macrophages were analyzed by flow cytometry as described in the materials and methods and supplementary information. Total number of (A) $CD45^+$ cells, (B) $CD11b^+$ cells, (C) neutrophils and (D) eosinophils in colonic tissue from each group. (E) Representative dot plots from control, CAC control and CAC+iMSCs mice showing the $F4/80^+$ monocyte-macrophage differentiation waterfall. Total number of (F) immature $CD86^+$ macrophages, (G) $Ly6C^{hi}MHCII^-$, (H) $Ly6C^-MHCII^+$ monocytes and, (I) mature $Ly6C^-MHCII^+CD206^+$ macrophages in the three experimental groups. Box plots represent ± SEM range, median (middle line) and extreme values (whiskers). Graphs without letters reflect no significant differences between groups.

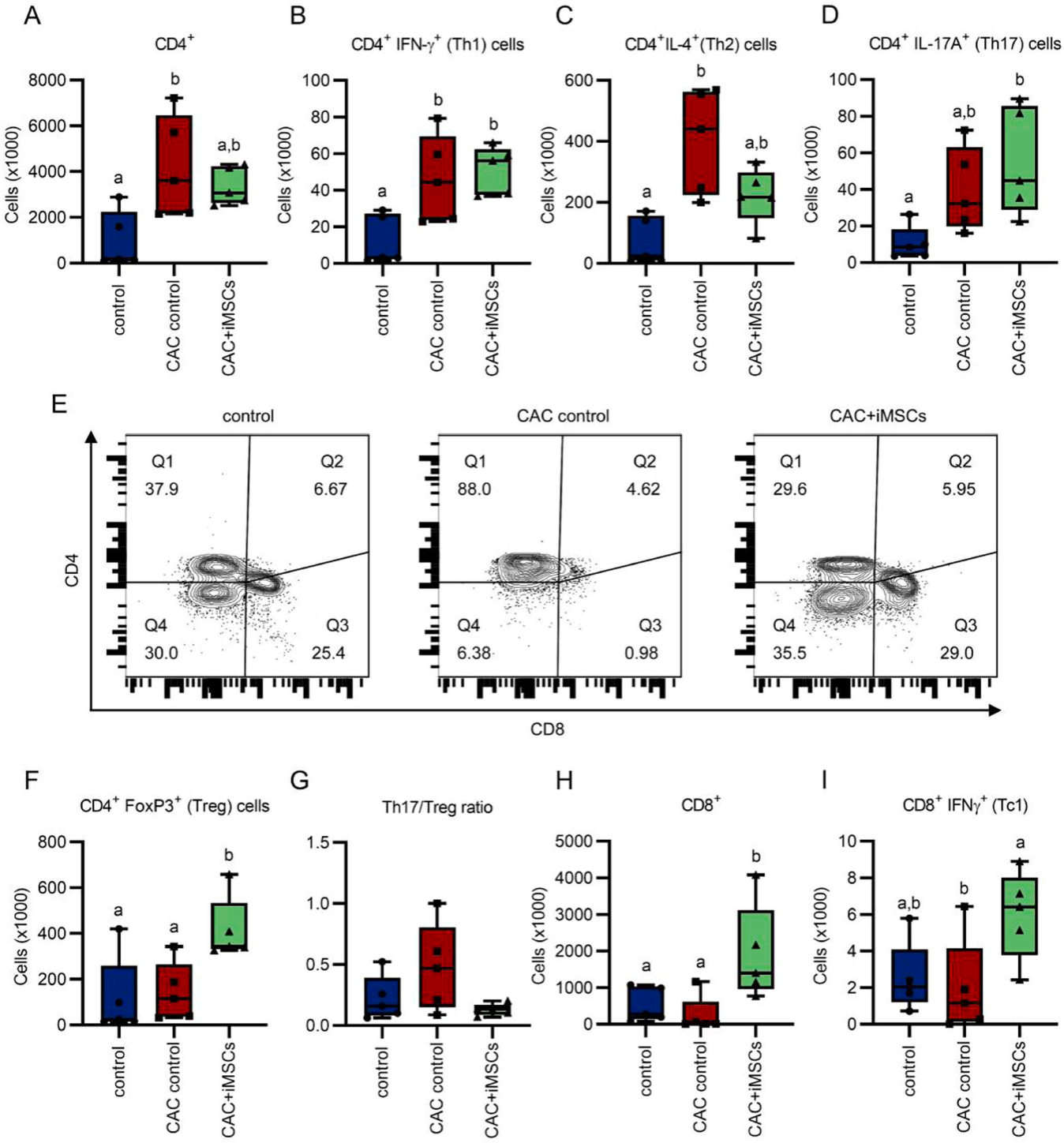


**Fig. 7.** iMSC administrations modulate the T cell response in MLNs of AOM/DSS mice. MLNs from control, CAC control and CAC+iMSCs mice (n = 5 mice/group) were collected at the end of the experiment, T cell populations were analyzed by flow cytometry as described in the materials and methods and supplementary information. (A) Total $CD3^+CD4^+$ T cells, (B) Th1 ($CD4^+IFN\text{-}\gamma^+$), (C) Th2 ($CD4^+IL\text{-}4^+$), (D) Th17 ($CD4^+IL\text{-}17A^+$) and (F) $CD4^+FoxP3^+$Tregs in control, CAC control, and CAC+iMSCs mice. (E) Representative dot plots from control, CAC control and CAC+iMSCs mice showing the CD4 vs. CD8 T lymphocyte distribution. (G) Th17/Treg ratio from the previous data. (H) Total $CD3^+CD8^+$ and (I) Tc1 ($CD8^+IFN\text{-}\gamma^+$) cells. Box plots represent ± SEM range, median (middle line) and extreme values (whiskers). Groups with different letters (a-b) exhibit statistically significant differences ($P < 0.05$). Graphs without letters reflect no significant differences between groups.

## 4. Discussion

To date only a few studies have analyzed the effects of non-genetically modified syn-, allo- and xenogeneic MSCs on tumor induction/growth and immune responses in rodent models of CAC, with varying protocols and outcomes (Supplementary Fig. 1). To study the effect of human iMSCs on CAC, we used the AOM/DSS model where macroscopically visible lesions can be observed from week 3–4 after disease induction [15]. As MSCs have been shown to home to tumors and promote tumor growth, we injected iMSCs at the disease peaks of

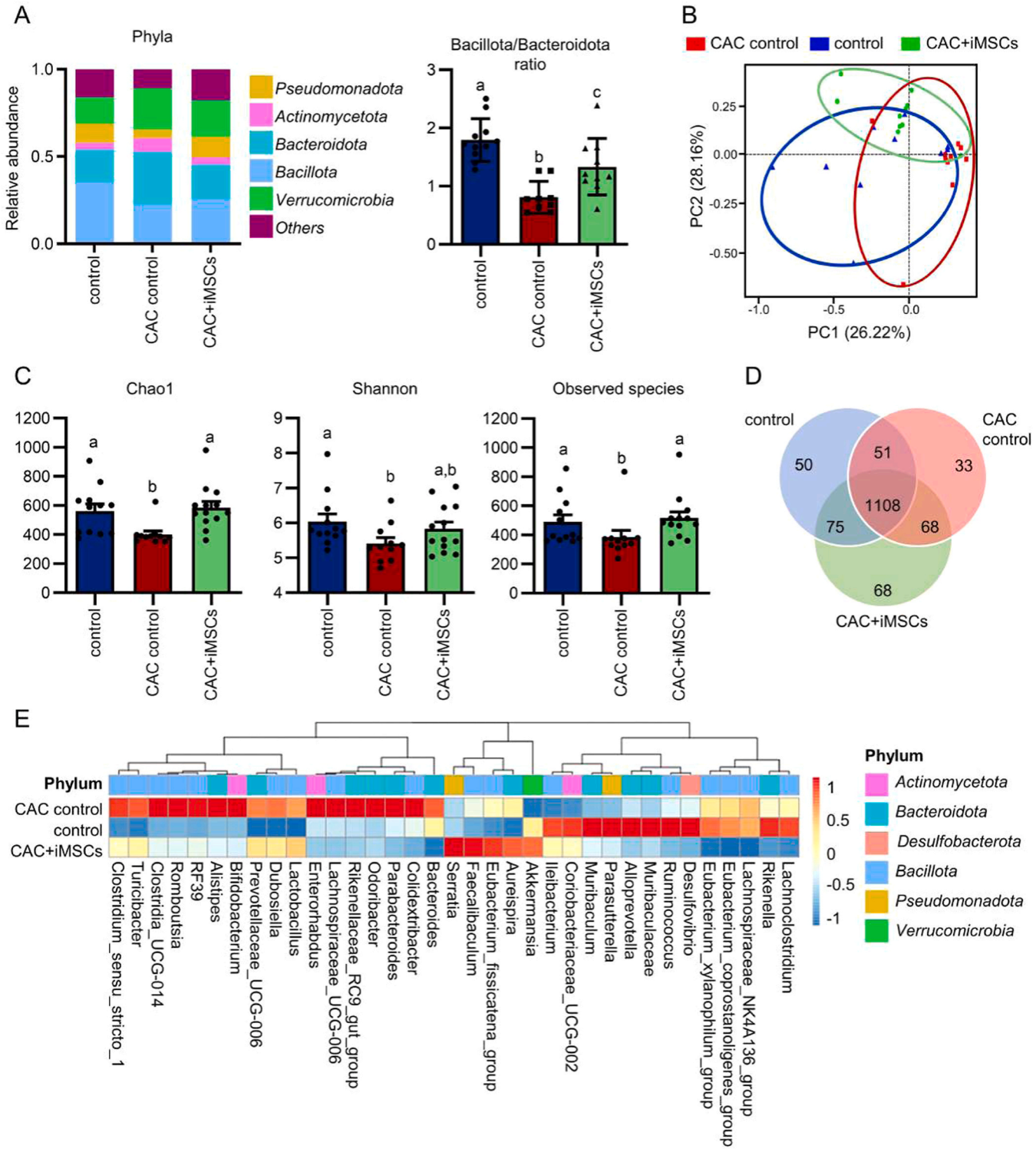


**Fig. 8.** Administrations of iMSCs partially restore the intestinal dysbiosis induced by the CAC**.** The fecal microbiota in control, CAC control and CAC+iMSCs groups was evaluated by Illumina sequencing. (A) Distribution histogram of relative abundance of taxa (left) and Bacillota/Bateroidota ratio (right), (B) β-diversity by principal coordinate analysis score plot, and microbiome diversity by (C) Chao1 richness (left), Shannon diversity (middle) and Observed OTUs (right). (D) A Venn diagram showing the number of OTUs which are unique and common to each experimental group. (E) A heatmap showing the taxonomic signatures at the genus level. Genera with average abundance levels > 0.5% (35 genera) in the three groups (control, CAC control and CAC+iMSCs) were used to construct the heatmap. Data are expressed as mean(SEM). Groups with different letters (a-b) exhibit statistically significant differences ($P < 0.05$). Graphs without letters reflect no significant differences between groups. OTU: operational taxonomic unit.

the second (week 4–5) and third DSS administration (week 7–8), i.e., at a time when visible lesions are already present. Our data show that the iMSCs administrations significantly inhibited the tumor number, as did the first-line colorectal cancer chemotherapeutic drug 5-FU, and in contrast to other studies we also detected a significant decrease in tumor size [18,21,34,36]. However, we did not detect the injected iMSCs in the intestine/tumors at the time of sacrifice (seven weeks after the last injection), which is consistent with their rapid disappearance and limited engraftment in mouse models [48] and in human patients [49]. In fact, some studies have shown that MSCs can inhibit intestinal inflammation without migrating to either the inflamed colon or the MLNs [50], which could be advantageous when employing MSCs for the treatment of IBD and its associated cancer. Importantly, the iMSCs did not adopt the pro-tumorigenic phenotype described by Hu and colleagues [19], but instead inhibited intestinal inflammation and tumorigenesis. This was evidenced by the downregulation of inflammatory mediators and pro-tumorigenic signaling pathways, including COX-2, and CRC-associated LMW β-catenin. Interestingly, a recent study by Hu et al., showed that the administration of syngeneic BM-MSCs ($2 \times 10^6$ cells/injection), starting at the third DSS cycle followed by seven weekly MSCs injections, promoted tumor formation in AOM/DSS mice, whereas weekly administrations of MSCs from the first DSS cycle inhibited CAC [51]). These data indicate that the timing of MSC-treatment can decide whether MSCs inhibit or promote tumor growth in the AOM/DSS-induced CAC model. Nevertheless, in contrast to the study by Hu and colleagues, we injected fewer MSCs ($0.5 \times 10^6$), and only during the end of the second and third DSS cycle, suggesting that repeated high-dose administrations of MSCs should be used cautiously when treating IBD.

In CRC, macrophages, and granulocytes in the tumor microenvironment produce reactive oxygen and nitrogen species that can cause DNA damage and mutations [52]. In steady state, Ly6C$^{hi}$MHCII$^-$ monocytes are recruited to the intestine and promptly differentiate into mature tissue resident Ly6C$^-$MHCII$^+$ monocytes through a monocyte-macrophage differentiation waterfall [42]. However, in CAC this process is disrupted, resulting in the accumulation of proinflammatory Ly6C$^{hi}$MHCII$^-$ monocytes/macrophages in the intestine [45]. Our data show that administration of iMSCs reduces the high numbers of circulating monocytes while promoting the maturation of intestinal Ly6C$^-$MHCII$^+$ macrophages, partially restoring the monocyte "waterfall". This was also reflected in a decrease in immature CD86$^+$ M1-like monocytes in the colons of iMSC-treated mice.

In recent years it has become clear that neutrophils play an important role in promoting tumorigenesis. Shang et al. showed that the progression of CAC in the AOM/DSS model was accompanied by an increased infiltration of neutrophils expressing CXCR2 into the colonic submucosa. Injection of neutrophil-neutralizing antibodies after the last DSS cycle reduced the number and size of tumors [53]. In addition, IL-17 promotes the activation and accumulation of neutrophils at sites of inflammation [54]. In accordance, we observed a marked decrease in the numbers of neutrophils in the colons of iMSC-treated mice in comparison to CAC mice, which correlated with the mRNA levels of IL-17 in each group. Apart from neutrophils, eosinophils are thought to play a major proinflammatory role in IBD and are increased in the intestinal mucosa in both CD and UC patients [43]. Polosukhina et al. demonstrated that DSS-administration induced a significant increase in colonic eosinophils in colitic mice compared to control mice. Furthermore, AOM/DSS-treated mice, lacking the eosinophil chemoattractant CCL11, had decreased histological injury, fewer tumors, and a reduced colonic eosinophil infiltration in comparison to wild type mice [55]. In accordance, we found that the administration of iMSCs decreased the number of eosinophils in CAC mice.

In summary, we have shown that iMSCs can partially restore normal intestinal macrophage differentiation in the intestine and reduce the infiltration of both neutrophils and eosinophils into the inflamed colons of AOM/DSS-treated mice. Interestingly, Lopez-Santalla et al. recently showed that the beneficial effects of administration of allogeneic ASCs in colitic mice were maintained over time, mainly due to the imprinting of an innate memory-like response in treated mice [56].

MSCs inhibit experimental colitis in part through the increase of FoxP3$^+$Tregs in MLNs and the inflamed colon [10]. Similarly, local injections of MSCs into patients suffering from fistulizing Crohn's disease increased the percentage of FoxP3$^+$ Tregs in blood and colonic mucosa, which was maintained up to 12 months after treatment [57]. In CAC, Tregs appear to play anti- or protumorigenic role depending on the stage of the disease. Using the AOM/DSS model, Pastille et al. showed that in vivo depletion of Tregs during the acute inflammation phase (i.e., during the first DSS cycle) resulted in a hyper aggressive intestinal inflammation. However, ablation of Tregs during the third DSS cycle increased the percentage of IFN-γ$^+$CD8$^+$ T cells in MLNs and colon which correlated with a decrease in tumor number/size [58]. These data suggest that Treg activity is beneficial during the initiation/induction phase of CAC, through their inhibition of inflammation, but promote the growth of established tumors by inhibiting anti-tumor immune responses mediated, in part, by IFN-γ$^+$CD8$^+$ T cells.

Tang et al. showed that administration of human umbilical cord MSCs during the first and second DSS cycle could suppress AOM/DSS-induced CAC, which correlated with an increased accumulation of FoxP3$^+$ Tregs in the MLNs and colonic tissue [35]. In our study, we adopted a late treatment protocol, starting at the end of the second DSS cycle when visible lesions should be present. This treatment modality could be representative of cases where MSCs are given to IBD patients with undiagnosed premalignant lesions, risking a Treg-mediated promotion of tumorigenesis. However, we did not observe any tumor-promoting activities of the iMSCs, despite the induction of a persistent immunosuppressive response (highlighted by the significantly lower DAI score in the CAC+iMSCs group during the third DSS cycle), and a significant increase in the numbers of FoxP3$^+$ T cells in the MLNs. Interestingly, we observed that iMSC-treatments induced a significant increase of CD8$^+$ T cells, including IFN-γ-producing CD8$^+$ T cells, in the MLNs, despite the increase in Tregs. We hypothesize that iMSCs can suppress inflammation, probably via Tregs and immunosuppressive myeloid cell populations, while simultaneously permitting anti-tumor immune responses by CD8$^+$ T cells.

Regarding the Th2 subset, Spinner et al. recently showed that Th2 cells promote tumor progression in the AOM/DSS model. Blocking the Th2 response resulted in an increased Th1/Th17/Tc response which reduced the colitis-associated tumorigenesis [59]. In our study, we observed a decrease in CD4$^+$IL-4$^+$ Th2 cells in parallel with an increase in CD4$^+$IL-17A$^+$ Th17 cells in the MLNs of iMSC-treated mice in comparison to CAC control mice. This is in contrast with Tang et al. [35] who showed that MSCs increased Tregs in MLN while not affecting Th2 and Th17 cells. Furthermore, while the reduction of the Th2 responses fits well with the inhibition of tumorigenesis in iMSC-treated mice, the increase of the Th17 compartment is harder to explain since these cells have been implicated in tumor progression in CAC [60]. This could be because Tregs highly outnumbered the Th17 cells in MLNs. In fact, the Th17/Treg ratio in iMSCs-treated mice is similar to that found in healthy control mice. Thus, we believe that Tregs activated in the MLNs can sufficiently control the expansion of the Th17 compartment in the colon.

Controlled interactions between the commensal gut microbiota and host immunity are key in ensuring immunological homeostasis in the intestine. Alterations of the composition of the microbiota are associated with several pathologies, including IBD and CRC, and represent a promising therapeutic target [20]. More specifically, a decrease of the Bacillota/Bacteroidota ratio is widely regarded as dysbiosis. Accordingly, a reduction in bacteria belonging to the *Bacillota* phyla, such as *Ruminococcus* and an increase in the abundance of *Bacteroidota*, *Actinomycetota* and *Verrucomicrobia* have been observed in both experimental models and clinical studies of colitis and CRC [61,62].

We have shown that CAC control mice exhibited a significantly reduced Bacillota/Bacteroidota ratio compared with control mice, which is in line with several studies using the AOM/DSS model of CAC

[63]. Interestingly, the administrations of iMSCs were able to significantly increase the Bacillota/Bacteroidota ratio, although these data do not agree with a previous study that found a reduction in the Bacillota/Bacteroidota ratio in the BM-MSC-treated CAC mice [21]. Moreover, in our study, iMSC-treatment elevated both the α-diversity (Shannon's diversity and Chao1 indexes) and β-diversity (PCoA analysis), while He at al. only found a significant restoration of the β-diversity [21]. These discrepancies could be due to differences in the experimental setup, such as the timing of MSC administrations, the fecal sampling, and the gender of the mice used [64].

Lastly, the higher abundance of different bacterial genera is consistent with previous reported studies. In fact, *Bacteroides* has been positively correlated with inflammatory factors and negatively correlated with intestinal barrier integrity [65], as well as playing an important role in triggering colitis [66]. Similarly, the MSC-treatment decreased the AOM/DSS-induced increase of *Turicibacter* and *Alistipes,* two pro-inflammatory bacteria that are abundant in CAC mice [17,67]. The iMSCs treatment was also able to partially restore all genera modified in the CAC control group. Conversely, iMSC treatment increased *Akkermansia,* which is associated with a healthy gut microbiota [17] and can protect against colitis and CAC [68,69]. Consequently, it is conceivable that the underlying mechanisms implicated in the beneficial effect of the iMSCs treatment will be the mutualistic relationship between the "new" microbiota composition and the host immune system.

It needs to be pointed out that we have evaluated the human iMSCs in a xenogeneic setting since some reports have highlighted species incompatibilities that prevent the proper evaluation of human MSCs in rodent models. However, key molecules important for the immunomodulatory ($PGE_2$, IL-10 and TGF-β1) and homing capacities (SDF-1/CXCR4) of MSCs are cross-reactive between human and mouse [70,71]. Furthermore, the immunomodulatory, tissue regenerative and homing properties of human MSCs have been successfully evaluated in multiple xenogeneic mouse models of disease, comparable to those of murine MSCs [72]. These data suggest that xenogeneic models for the evaluation of human MSCs are valid and robust.

## 5. Conclusion

We have shown that late administrations of iMSCs induce a sustained inhibition of intestinal inflammation, characterized by a reduced infiltration of innate immune cells, a modulation of the adaptive immune response, and amelioration of the intestinal dysbiosis, resulting in a significant decrease in tumor number and size. Our data support the systemic application of MSC for the treatment of IBD, providing a benefit in preventing CAC.

## Ethics approval and consent to participate

This study was conducted under the Helsinki Declaration of 1975. All patients provided written informed consent before enrollment, and the study was approved by the Research Ethics Committee of Granada, Andalusian Public Sanitary System, Spain.

All animal experimental procedures were approved by the Ethics Committee of Laboratory Animals of the University of Granada (Spain) (CEEA 17/09/2019/156) and followed the "Guide for the Care and Use of Laboratory Animals" as promulgated by the National Institute of Health.

## CRediT authorship contribution statement

**Laura Hidalgo-García**: Conceptualization, Formal analysis, Investigation, Methodology Validation, Visualization, Roles/Writing - original draft, Writing - review & editing. **Antonio Jesús Ruiz-Malagon**: Conceptualization, Formal analysis, Investigation, Methodology Validation, Writing - review & editing. **Francisco Huertas**: Methodology, Resources, Writing - review & editing. **María Jesús Rodríguez-Sojo**: Formal analysis, Investigation, Methodology, Writing - review & editing. **José Alberto Molina-Tijeras**: Formal analysis, Investigation, Methodology, Writing - review & editing. **Patricia Diez-Echave**: Formal analysis, Investigation, Methodology, Writing - review & editing. **Patricia Becerra**: Methodology, Investigation, Writing - review & editing. **Benito Mirón**: Methodology, Resources, Writing - review & editing. **Rocío Morón**: Methodology, Supervision, Writing - review & editing. **Alba Rodríguez-Nogales:** Conceptualization, Formal analysis, Investigation, Methodology, Validation, Visualization, Funding acquisition, Roles/Writing - original draft, Writing - review & editing. **Julio Gálvez**: Conceptualization, Validation, Funding acquisition, Supervision, Project administration, Roles/Writing - original draft, Writing - review & editing. **María Elena Rodríguez-Cabezas**: Conceptualization, Methodology, Validation, Funding acquisition, Supervision, Project administration, Roles/Writing - original draft, Writing - review & editing. **Per Anderson**: Conceptualization, Validation, Funding acquisition, Supervision, Roles/Writing - original draft, Writing - review & editing.

## Declaration of Competing Interest

The authors have no conflicts of interest to declare.

## Data availability

Data will be made available on request.

## Acknowledgments and Funding

This article has been funded by the Instituto de Salud Carlos III (ISCIII) (Spain) through the Project PI22/01630 and cofounded by the European Union. This work was also supported by the Junta de Andalucía (CTS 164) (Spain), and Fondo Europeo de Desarrollo Regional (FEDER), from the European Union, through the CIBer-EHD and the research grants PI18/00826, P18-RT-4930, PI0206–2016, and PI19/01058. L. H-G and A.J. R-M are predoctoral fellows funded by the Spanish Ministry of Science and Innovation ("Programa de Doctorado: Medicina Clínica y Salud Pública" B12.56.1). J.A. M-T and M.J. R-S are predoctoral fellows from the Instituto de Salud Carlos III (FI17/00176). P. D-E is a postdoctoral fellow of Junta de Andalucía (P18-RT-4930). P.A is supported by the Consejería de Salud, Junta de Andalucía through the contract "Nicolás Monardes" (C-0013–2018). A. R-N is a postdoctoral fellow from the Instituto de Salud Carlos III (Miguel Servet program (CP19/00191).

*Contributions*

LHG, JG, RM, ARN, MERC and PA designed and analyzed experiments. LHG, AJRM, MJRS, JAMT and PDE performed experiments. FH and BM provided human samples. PB did pathologic analysis. PA, MERC, JG and ARN wrote the manuscript. All authors read and approved the final manuscript.

*Consent for publication*

Not applicable.

## Appendix A. Supporting information

Supplementary data associated with this article can be found in the online version at doi:10.1016/j.phrs.2023.106891.

## References

1 Collaborators GIBD The global, regional, and national burden of inflammatory bowel disease in 195 countries and territories, 1990–2017: a systematic analysis for the Global Burden of Disease Study 2017. Lancet Gastroenterol Hepatol. 2019 Jan;5(1): 17–30.

2 M. Sun, C. He, Y. Cong, Z. Liu, Regulatory immune cells in regulation of intestinal inflammatory response to microbiota, Mucosal Immunol. 8 (5) (2015) 969–978.
3 C.R. Choi, I. Al Bakir, N.J. Ding, G.H. Lee, A. Askari, J. Warusavitarne, et al., Cumulative burden of inflammation predicts colorectal neoplasia risk in ulcerative colitis: a large single-centre study, Gut 68 (3) (2019) 414–422.
4 J.A. Eaden, K.R. Abrams, J.F. Mayberry, The risk of colorectal cancer in ulcerative colitis: a meta-analysis, Gut 48 (4) (2001) 526–535.
5 B. Ou, J. Zhao, S. Guan, A. Lu, Survival of colorectal cancer in patients with or without inflammatory bowel disease: a meta-analysis, Dig. Dis. Sci. 61 (3) (2016) 881–889.
6 M.C. Mattar, D. Lough, M.J. Pishvaian, A. Charabaty, Current management of inflammatory bowel disease and colorectal cancer, Gastrointest. Cancer Res 4 (2) (2011) 53–61.
7 M. Alkhayyat, M. Abureesh, A. Gill, G. Khoudari, M. Abou Saleh, E. Mansoor, et al., Lower rates of colorectal cancer in patients with inflammatory bowel disease using anti-TNF therapy, Inflamm. Bowel Dis. 27 (7) (2021&;;) 1052–1060.
8 M. Lemaitre, J. Kirchgesner, A. Rudnichi, F. Carrat, M. Zureik, F. Carbonnel, et al., Association between use of thiopurines or tumor necrosis factor antagonists alone or in combination and risk of lymphoma in patients with inflammatory bowel disease, JAMA 318 (17) (2017) 1679–1686.
9 M. Crisan, S. Yap, L. Casteilla, C.W. Chen, M. Corselli, T.S. Park, et al., A perivascular origin for mesenchymal stem cells in multiple human organs, Cell Stem Cell 3 (3) (2008) 301–313.
10 E. Gonzalez-Rey, P. Anderson, M.A. Gonzalez, L. Rico, D. Buscher, M. Delgado, Human adult stem cells derived from adipose tissue protect against experimental colitis and sepsis, Gut 58 (7) (2009) 929–939.
11 J. Panes, D. Garcia-Olmo, G. Van Assche, J.F. Colombel, W. Reinisch, D.C. Baumgart, et al., Expanded allogeneic adipose-derived mesenchymal stem cells (Cx601) for complex perianal fistulas in Crohn's disease: a phase 3 randomised, double-blind controlled trial, Lancet 388 (10051) (2016) 1281–1290.
12 Li, G.C. Zhang, H.W. Zhao, Q.C. Sun LI, J.J. Yang, L. Hong, et al., Mesenchymal stem cells promote tumor angiogenesis via the action of transforming growth factor beta1, Oncol. Lett. 11 (2) (2016) 1089–1094.
13 Y. Zhang, A. Daquinag, D.O. Traktuev, F. Amaya-Manzanares, P.J. Simmons, K. L. March, et al., White adipose tissue cells are recruited by experimental tumors and promote cancer progression in mouse models, Cancer Res. 69 (12) (2009) 5259–5266.
14 J.H. Li, W.S. Fan, M.M. Wang, Y.H. Wang, Z.G. Ren, Effects of mesenchymal stem cells on solid tumor metastasis in experimental cancer models: a systematic review and meta-analysis, J. Transl. Med. 16 (1) (2018) 113.
15 C. Neufert, C. Heichler, T. Brabletz, K. Scheibe, V. Boonsanay, F.R. Greten, et al., Inducible mouse models of colon cancer for the analysis of sporadic and inflammation-driven tumor progression and lymph node metastasis, Nat. Protoc. 16 (1) (2021) 61–85.
16 M. Takahashi, K. Wakabayashi, Gene mutations and altered gene expression in azoxymethane-induced colon carcinogenesis in rodents, Cancer Sci. 95 (6) (2004) 475–480.
17 Y. Chung, Y. Ryu, B.C. An, Y.S. Yoon, O. Choi, T.Y. Kim, et al., A synthetic probiotic engineered for colorectal cancer therapy modulates gut microbiota, Microbiome 9 (1) (2021), 122.
18 M. Nasuno, Y. Arimura, K. Nagaishi, H. Isshiki, K. Onodera, S. Nakagaki, et al., Mesenchymal stem cells cancel azoxymethane-induced tumor initiation, Stem Cells 32 (4) (2014) 913–925.
19 S. Hu, J. Yuan, J. Xu, X. Li, G. Zhang, Q. Ma, et al., TNF-alpha and IFN-gamma synergistically inhibit the repairing ability of mesenchymal stem cells on mice colitis and colon cancer, Am. J. Transl. Res. 11 (9) (2019) 6207–6220.
20 Y. Cheng, Z. Ling, L. Li, The intestinal microbiota and colorectal cancer, Front. Immunol. 11 (2020), 615056.
21 R. He, C. Han, Y. Li, W. Qian, X. Hou, Cancer-preventive role of bone marrow-derived mesenchymal stem cells on colitis-associated colorectal cancer: roles of gut microbiota involved, Front. Cell Dev. Biol. 9 (2021), 642948.
22 L. Hidalgo-Garcia, J.A. Molina-Tijeras, F. Huertas-Pena, A.J. Ruiz-Malagon, P. Diez-Echave, T. Vezza, et al., Intestinal mesenchymal cells regulate immune responses and promote epithelial regeneration in vitro and in dextran sulfate sodium-induced experimental colitis in mice, Acta Physiol. 233 (2) (2021), e13699.
23 J. Garrido-Mesa, A. Rodriguez-Nogales, F. Algieri, T. Vezza, L. Hidalgo-Garcia, M. Garrido-Barros, et al., Immunomodulatory tetracyclines shape the intestinal inflammatory response inducing mucosal healing and resolution, Br. J. Pharmacol. 175 (23) (2018) 4353–4370.
24 C. Becker, M.C. Fantini, M.F. Neurath, High resolution colonoscopy in live mice, Nat. Protoc. 1 (6) (2006) 2900–2904.
25 A. Rodriguez-Nogales, F. Algieri, J. Garrido-Mesa, T. Vezza, M.P. Utrilla, N. Chueca, et al., Differential intestinal anti-inflammatory effects of Lactobacillus fermentum and Lactobacillus salivarius in DSS mouse colitis: impact on microRNAs expression and microbiota composition, Mol. Nutr. Food Res 61 (11) (2017).
26 T. Magoc, S.L. Salzberg, FLASH: fast length adjustment of short reads to improve genome assemblies, Bioinformatics 27 (21) (2011) 2957–2963.
27 N.A. Bokulich, S. Subramanian, J.J. Faith, D. Gevers, J.I. Gordon, R. Knight, et al., Quality-filtering vastly improves diversity estimates from Illumina amplicon sequencing, Nat. Methods 10 (1) (2013) 57–59.
28 J.G. Caporaso, J. Kuczynski, J. Stombaugh, K. Bittinger, F.D. Bushman, E.K. Costello, et al., QIIME allows analysis of high-throughput community sequencing data, Nat. Methods 7 (5) (2010) 335–336.
29 R.C. Edgar, B.J. Haas, J.C. Clemente, C. Quince, R. Knight, UCHIME improves sensitivity and speed of chimera detection, Bioinformatics 27 (16) (2011) 2194–2200.
30 B.J. Haas, D. Gevers, A.M. Earl, M. Feldgarden, D.V. Ward, G. Giannoukos, et al., Chimeric 16S rRNA sequence formation and detection in Sanger and 454-pyrosequenced PCR amplicons, Genome Res 21 (3) (2011) 494–504.
31 R.C. Edgar, UPARSE: highly accurate OTU sequences from microbial amplicon reads, Nat. Methods 10 (10) (2013) 996–998.
32 Q. Wang, G.M. Garrity, J.M. Tiedje, J.R. Cole, Naive Bayesian classifier for rapid assignment of rRNA sequences into the new bacterial taxonomy, Appl. Environ. Microbiol 73 (16) (2007) 5261–5267.
33 C. Quast, E. Pruesse, P. Yilmaz, J. Gerken, T. Schweer, P. Yarza, et al., The SILVA ribosomal RNA gene database project: improved data processing and web-based tools, Nucleic Acids Res. 41 (Database issue) (2013) D590–D596.
34 Z. Chen, X. He, X. Chen, X. Lin, Y. Zou, X. Wu, et al., Bone marrow mesenchymal stem cells ameliorate colitis-associated tumorigenesis in mice, Biochem Biophys. Res. Commun. 450 (4) (2014) 1402–1408.
35 R.J. Tang, S.N. Shen, X.Y. Zhao, Y.Z. Nie, Y.J. Xu, J. Ren, et al., Mesenchymal stem cells-regulated Treg cells suppress colitis-associated colorectal cancer, Stem Cell Res Ther. 6 (2015), 71.
36 X.B. Zheng, X.W. He, L.J. Zhang, H.B. Qin, X.T. Lin, X.H. Liu, et al., Bone marrow-derived CXCR4-overexpressing MSCs display increased homing to intestine and ameliorate colitis-associated tumorigenesis in mice, Gastroenterol. Rep. 7 (2) (2019) 127–138.
37 S. Grivennikov, E. Karin, J. Terzic, D. Mucida, G.Y. Yu, S. Vallabhapurapu, et al., IL-6 and Stat3 are required for survival of intestinal epithelial cells and development of colitis-associated cancer, Cancer Cell 15 (2) (2009) 103–113.
38 M. Jary, R. Hasanova, A. Vienot, K. Asgarov, R. Loyon, C. Tirole, et al., Molecular description of ANGPT2 associated colorectal carcinoma, Int. J. Cancer 147 (7) (2020) 2007–2018.
39 J.L. Langowski, X. Zhang, L. Wu, J.D. Mattson, T. Chen, K. Smith, et al., IL-23 promotes tumour incidence and growth, Nature 442 (7101) (2006) 461–465.
40 T. Goretsky, E.M. Bradford, Q. Ye, O.F. Lamping, T. Vanagunas, M.P. Moyer, et al., Beta-catenin cleavage enhances transcriptional activation, Sci. Rep. 8 (1) (2018), 671.
41 Y. Yang, L. Li, C. Xu, Y. Wang, Z. Wang, M. Chen, et al., Cross-talk between the gut microbiota and monocyte-like macrophages mediates an inflammatory response to promote colitis-associated tumourigenesis, Gut (2020).
42 T. Joeris, K. Muller-Luda, W.W. Agace, A.M. Mowat, Diversity and functions of intestinal mononuclear phagocytes, Mucosal Immunol. 10 (4) (2017) 845–864.
43 T. Alhmoud, A. Gremida, D. Colom Steele, I. Fallahi, W. Tuqan, N. Nandy, et al., Outcomes of inflammatory bowel disease in patients with eosinophil-predominant colonic inflammation, BMJ Open Gastroenterol. 7 (1) (2020), e000373.
44 C.C. Hedrick, I. Malanchi, Neutrophils in cancer: heterogeneous and multifaceted, Nat. Rev. Immunol. 22 (3) (2022) 173–187.
45 C.C. Bain, C.L. Scott, H. Uronen-Hansson, S. Gudjonsson, O. Jansson, O. Grip, et al., Resident and pro-inflammatory macrophages in the colon represent alternative context-dependent fates of the same Ly6Chi monocyte precursors, Mucosal Immunol. 6 (3) (2013) 498–510.
46 N. Eastaff-Leung, N. Mabarrack, A. Barbour, A. Cummins, S. Barry, Foxp3+ regulatory T cells, Th17 effector cells, and cytokine environment in inflammatory bowel disease, J. Clin. Immunol. 30 (1) (2010) 80–89.
47 M.J. Waldner, M.F. Neurath, Mechanisms of immune signaling in colitis-associated cancer, Cell Mol. Gastroenterol. Hepatol. 1 (1) (2014) 6–16.
48 P. Yin, L. Gui, C. Wang, J. Yan, M. Liu, L. Ji, et al., Targeted delivery of CXCL9 and OX40L by mesenchymal stem cells elicits potent antitumor immunity, Mol. Ther. 28 (12) (2020) 2553–2563.
49 L. von Bahr, I. Batsis, G. Moll, M. Hagg, A. Szakos, B. Sundberg, et al., Analysis of tissues following mesenchymal stromal cell therapy in humans indicates limited long-term engraftment and no ectopic tissue formation, Stem Cells 30 (7) (2012) 1575–1578.
50 L. Hidalgo-Garcia, J. Galvez, M.E. Rodriguez-Cabezas, P.O. Anderson, Can a conversation between mesenchymal stromal cells and macrophages solve the crisis in the inflamed intestine? Front Pharmacol. 9 (2018), 179.
51 W. Hu, W. Wang, X. Jiang, Z. Wang, R. Lin, Mesenchymal stem cells can prevent or promote the progression of colon cancer based on their timing of administration, J. Transl. Med 21 (1) (2023), 227.
52 J. Kay, E. Thadhani, L. Samson, B. Engelward, Inflammation-induced DNA damage, mutations and cancer, DNA Repair 83 (2019), 102673.
53 K. Shang, Y.P. Bai, C. Wang, Z. Wang, H.Y. Gu, X. Du, et al., Crucial involvement of tumor-associated neutrophils in the regulation of chronic colitis-associated carcinogenesis in mice, PLOS One 7 (12) (2012), e51848.
54 D. He, H. Li, N. Yusuf, C.A. Elmets, J. Li, J.D. Mountz, et al., IL-17 promotes tumor development through the induction of tumor promoting microenvironments at tumor sites and myeloid-derived suppressor cells, J. Immunol. 184 (5) (2010) 2281–2288.
55 D. Polosukhina, K. Singh, M. Asim, D.P. Barry, M.M. Allaman, D.M. Hardbower, et al., CCL11 exacerbates colitis and inflammation-associated colon tumorigenesis, Oncogene 40 (47) (2021) 6540–6546.
56 M. Lopez-Santalla, R. Hervas-Salcedo, M. Fernandez-Garcia, J.A. Bueren, M.I. Garin, Cell therapy with mesenchymal stem cells induces an innate immune memory response that attenuates experimental colitis in the long term, J. Crohns Colitis 14 (10) (2020) 1424–1435.
57 R. Ciccocioppo, M.E. Bernardo, A. Sgarella, R. Maccario, M.A. Avanzini, C. Ubezio, et al., Autologous bone marrow-derived mesenchymal stromal cells in the treatment of fistulising Crohn's disease, Gut 60 (6) (2011) 788–798.
58 E. Pastille, K. Bardini, D. Fleissner, A. Adamczyk, A. Frede, M. Wadwa, et al., Transient ablation of regulatory T cells improves antitumor immunity in colitis-associated colon cancer, Cancer Res 74 (16) (2014) 4258–4269.

59 C.A. Spinner, I. Lamsoul, A. Metais, C. Febrissy, C. Moog-Lutz, P.G. Lutz, The E3 ubiquitin ligase Asb2alpha in T helper 2 cells negatively regulates antitumor immunity in colorectal cancer, Cancer Immunol. Res. 7 (8) (2019) 1332–1344.
60 S.I. Grivennikov, K. Wang, D. Mucida, C.A. Stewart, B. Schnabl, D. Jauch, et al., Adenoma-linked barrier defects and microbial products drive IL-23/IL-17-mediated tumour growth, Nature 491 (7423) (2012) 254–258.
61 B. Flemer, D.B. Lynch, J.M. Brown, I.B. Jeffery, F.J. Ryan, M.J. Claesson, et al., Tumour-associated and non-tumour-associated microbiota in colorectal cancer, Gut 66 (4) (2017) 633–643.
62 C.Z. Wang, C. Yu, X.D. Wen, L. Chen, C.F. Zhang, T. Calway, et al., American ginseng attenuates colitis-associated colon carcinogenesis in mice: impact on gut microbiota and metabolomics, Cancer Prev. Res 9 (10) (2016) 803–811.
63 M. Wang, B. Zhou, W. Cong, M. Zhang, Z. Li, Y. Li, et al., Amelioration of AOM/DSS-induced murine colitis-associated cancer by evodiamine intervention is primarily associated with gut microbiota-metabolism-inflammatory signaling axis, Front. Pharmacol. 12 (2021), 797605.
64 C.H. Song, N. Kim, R.H. Nam, S.I. Choi, J.E. Yu, H. Nho, et al., Changes in microbial community composition related to sex and colon cancer by Nrf2 knockout, Front. Cell Infect. Microbiol. 11 (2021), 636808.
65 G. Jin, Q. Tang, J. Ma, X. Liu, B. Zhou, Y. Sun, et al., Maternal emulsifier P80 intake induces gut dysbiosis in offspring and increases their susceptibility to colitis in adulthood, mSystems 6 (2) (2021).
66 T. Ohkusa, S. Koido, Intestinal microbiota and ulcerative colitis, J. Infect. Chemother. 21 (11) (2015) 761–768.
67 J.P. Zackular, N.T. Baxter, K.D. Iverson, W.D. Sadler, J.F. Petrosino, G.Y. Chen, et al., The gut microbiome modulates colon tumorigenesis, mBio 4 (6) (2013) (e00692-13).
68 X. Bian, W. Wu, L. Yang, L. Lv, Q. Wang, Y. Li, et al., Administration of akkermansia muciniphila ameliorates dextran sulfate sodium-induced ulcerative colitis in mice, Front. Microbiol. 10 (2019), 2259.
69 L. Wang, L. Tang, Y. Feng, S. Zhao, M. Han, C. Zhang, et al., A purified membrane protein from Akkermansia muciniphila or the pasteurised bacterium blunts colitis associated tumourigenesis by modulation of CD8(+) T cells in mice, Gut 69 (11) (2020) 1988–1997.
70 J.M. Hong, J.H. Kim, G.H. Kim, H.M. Shin, Y.I. Hwang, Xenogeneic humoral immune responses to human mesenchymal stem cells in mice, Int J. Stem Cells 15 (3) (2022) 291–300.
71 A. Peled, I. Petit, O. Kollet, M. Magid, T. Ponomaryov, T. Byk, et al., Dependence of human stem cell engraftment and repopulation of NOD/SCID mice on CXCR4, Science 283 (5403) (1999) 845–848.
72 Y.W. Won, A.N. Patel, D.A. Bull, Cell surface engineering to enhance mesenchymal stem cell migration toward an SDF-1 gradient, Biomaterials 35 (21) (2014) 5627–5635.